New Mass-Transfer Correlations for Packed Towers

Brian Hanley and Chau-Chyun Chen
Aspen Technology, Inc., Burlington, MA 01803

DOI 10.1002/aic.12574
Published online March 22, 2011 in Wiley Online Library (wileyonlinelibrary.com).

Rate-based calculations for trayed and packed columns offer process engineers a more rigorous and reliable basis for assessing column performance than the traditional equilibrium-stage approach, especially for multicomponent separations. Although the mathematics, thermodynamics, and transport-related physics upon which nonequilibrium separations theory is founded are generally true, it is also true that rate-based simulations today suffer from a serious weakness—they are ultimately tied to underlying equipment performance correlations with questionable predictive capability. In the case of packed columns operated countercurrently, correlations are required for the mass-transfer coefficients, k_x *and* k_y*, for the specific area participating in mass transfer,* a_m*, for the two-phase pressure drop,* $(\Delta p/Z)_{2\phi}$*, and for the flood capacity of the column. In particular, it is generally well known that packing mass-transfer correlations available in the public domain are unreliable when they are applied to chemical systems and column operating conditions outside of those used to develop the correlations in the first place. For that reason, we undertake the development of dependable, dimensionally consistent, correlating expressions for the mass-transfer-related quantities* k_x*,* k_y*, and* a_m *for metal Pall rings, metal IMTP, sheet metal structured packings of the MELLAPAK type, and metal gauze structured packings in the X configuration, using a new data fitting procedure. We demonstrate the superior performance of these correlations for a wide range of chemical systems and column operating conditions, including distillations as well as acid gas capture with amines. Further, we show that these new correlations lead to predictions for the relative interfacial area participating in mass transfer that can be greatly in excess of the geometrical surface area of the packing itself.* © 2011 American Institute of Chemical Engineers *AIChE J,* 58: 132–152, 2012

Keywords: mass-transfer coefficients, mass-transfer area, packed column, HETP, rate-based simulation

Introduction

Recently, the American Institute of Chemical Engineers, in conjunction with the US Department of Energy, published *Vision 2020: 2000 Separations Roadmap*.[1] This document outlines technical barriers and research needs for the foreseeable future in the areas of adsorption, extraction, crystallization, membranes, bioseparations, and distillation. Prominent among the most important research needs and barriers for distillation are as follows: (1) the need for a better understanding of mass transfer and multiphase flow in both trayed and packed columns, (2) the lack of accurate real-stage efficiency models for these types of columns, and (3) the fact that nonequilibrium column models lack accuracy, generality, and ease of use. In this article, we attempt to address some of the issues raised in the *Vision 2020* report

Correspondence concerning this article should be addressed to B. Hanley at brian.hanley@aspentech.com.

Table 1. Experimental Results from Kister[8] and Schultes[9]

System	Pressure (torr)	Packing	HETP (Billet)[5]	HETP (BF82)[4]	HETP (Onda)[3]	HETP (Aspen)	HETP (Expt)
C_6/n-C_7	760	2″ Pall ring	**43.2**	56	71.1	58.4	63–71[8]
1,2PG/EG	10	2″ Pall ring	**63.5**	**124.8**	**142.2**	106.7	96.5[8]
EB/SM	100	3½″ Pall ring	63.5	**126.2**	**142.2**	**55.9**	73.7[8]
EB/SM	100	1½″ Pall ring	**58.4**	46.8	43.2	45.8	40–48[8]
EB/SM	100	⅝″ Pall ring	40.6	31.2	**19**	33	28–38[8]
p/*o*-Xylene	50	⅝″ Pall ring	40.6	40.3	**17.1**	33	35–38[8]
i-C_4/n-C_4	8533	2″ Pall ring	**16.5**	51.5	53.3	48.3	51[9]
i-Octane/tol	760	1″ Pall ring	**24.6**	35	**21.3**	39.9	40.6[8]
i-Octane/tol	760	2″ Pall ring	**33**	60.1	**49.5**	**50**	66–71[8]
D_2O/H_2O	350	HY-PAK #1	**64.8**	**29.9**	**30.5**	**34.8**	48.2[8]

In all cases the countercurrent flow model was used. All experiments at total reflux. HETPs are reported in cm.
PG, propylene glycol; EG, ethylene glycol; EB, ethylbenzene; SM, styrene.

specifically related to the need for more accurate mass-transfer correlations in packed columns and the use of these types of correlations in rate-based simulation.

We begin by reviewing the performance of a few of the more commonly used packed-column mass-transfer correlations when they are used to predict the **H**eight **E**quivalent to a **T**heoretical **P**late (HETP) for binary separations. The HETP function for binary systems is particularly important to the development of packing mass-transfer correlations because it ties the separation performance of a tower expressed in terms of equilibrium stages to that column's performance expressed in terms of a rate-based differential contactor. In particular, we focus on several packed-column mass-transfer/interfacial-area correlations found in commercially available column simulation software like Aspen Technology's *Aspen Rate Based Distillation* component[2]: the equations of Onda et al.,[3] Bravo and Fair[4] (hereafter referred to as BF82), and Billet and Schultes[5] for random packings, the correlation of Bravo, Rocha, and Fair[6] for wire gauze structured packings (hereafter referred to as BRF85), and the correlations of Bravo, Rocha, and Fair[7] (hereafter referred to as BRF92) and of Billet and Schultes[5] for sheet metal structured packings. Table 1 is such a comparison for binary distillation experiments with random packings.[8,9] For each experimental system, we have calculated HETPs using the mass-transfer correlations for random packings listed above. As most distillations are primarily vapor phase controlled, the results in the table can be considered tests of the robustness of each correlation's $k_y a_m$ predictions (we expect $K_{Oy} \cong k_y$ for such systems). Calculated HETPs more than 20% different from the measured value range are bolded and underlined. Table 2 is a similar comparison for structured packings.[8,10–12] Once again, calculated HETPs more than 20% different than the measured value range are bolded and underlined. In Table 1, two-thirds of the calculated HETPs for random packings are more than 20% above or below the experimental values. In Table 2, about 40% of the predicted HETPs for structured packings are outside the ±20% envelope. These results clearly demonstrate that results generated during a rate-based simulation will often be limited by the reliability of the auxiliary mass/heat-transfer correlations needed to complete the mathematical description of the packed tower.

Mathematical Preliminaries

Before we turn to the development of specific mass-transfer correlations for random and structured packings, here we will first discuss several preliminary topics of interest primarily related to the proper interpretation of binary mass-transfer experiments using standard test mixtures.

The point HETP

The defining expression for the point HETP in a packed tower is developed by treating the packed tower as an equilibrium-stage contactor and then doing a mass balance over a single equilibrium stage (see, for example, Ref. 13). Normally, it is assumed that the major resistance to mass transfer resides in the vapor phase. Further, the development assumes that the equilibrium curve for the stage in question is straight for the composition changes encountered on the stage. For the sake of simplicity, we will assume here that constant molal overflow is true throughout the column. The assumption of constant molal overflow is almost always acceptable for analyzing binary distillation experiments with standard test mixtures that have small relative volatilities, α. The development below is strictly valid for binary systems. The equilibrium-stage concept is incompatible with the rate theory for mass transfer in multicomponent systems.[14]

Table 2. Experimental Results from Kister,[8] Fitz et al.,[10] Agrawal et al.,[11] and Kean et al.[12]

System	Pressure (torr)	Packing	HETP (Billet)[5]	HETP (BRF85)[6]	HETP (BF92)[7]	HETP (Aspen)	HETP (Expt)
Ar/O_2	1550	Flexipac 500Y	15.6	19.1	**22.1**	17.6	17.5[11]
p/*o*-Xylene	16	Mellapak 250Y	38.1	35.6	**50.8**	**43.2**	33.0[10]
p/*o*-Xylene	100	Flexipac 700Y	23.6	**9.1**	**14.7**	17.3	20.3[10]
CB/EB	76	Mellapak 350Y	29.2	24.8	**33.0**	27.4	26.7[8]
CB/EB	76	Mellapak 500Y	**30.5**	27.9	27.9	22.4	22.9[8]
i-C4/*n*-C4	8533	Mellapak 250Y	**11.9**	31.8	25.4	24.1	21.6–31[10]
C_6/n-C_7	1241	Flexipac 250Y	**21.8**	40.6	35.6	30.5	38–41[10]
cis-/*trans*-Decalin	304	Mellapak 250Y	**24.1**	41.9	39.4	38.1	33–35.6[8]
$TEG/H_2O/CH_4$	31,030	Flexipac 250Y	**472.4**	**348.0**	**1193.8**	140	167.6[12]

In all cases, the countercurrent flow model was used. All experiments at total reflux. HETPs are reported in cm.
CB, chlorobenzene; EB, ethylbenzene; TEG, triethylene glycol.

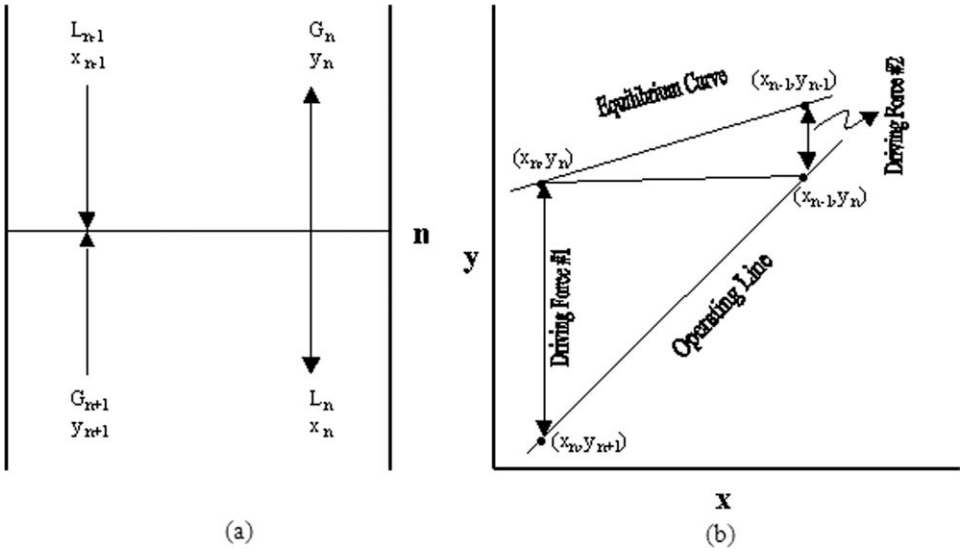

Figure 1. Diagram showing the changing driving force for mass transfer between the operating line and the equilibrium curve.

Consider the diagrams in Figure 1. Note that there is a continuously changing overall driving force for mass transfer. Where it is possible to assume that the equilibrium curve is linear over the range in which it is to be used, it can be shown that the logarithmic mean of the terminal potentials accounts for the continuously changing driving force exactly.[13,15]

The amount of the more volatile component (referred to as component "A") transferred from the vapor to the liquid phase per unit area (i.e., the flux of the more volatile component) is

$$N_{\mathrm{A}} = G(y_n - y_{n+1}) \tag{1}$$

where G is the molar flux of vapor in the column (assumed constant in the packed section because of constant molal overflow).

With the assumption that the equilibrium curve is straight

$$G(y_n - y_{n+1}) = (K_{\mathrm{Oy}} a_{\mathrm{m}})|_n \,\mathrm{HETP}_n \left(\frac{(y_n - y_{n+1}) - (y_{n-1} - y_n)}{\ln\left[\frac{y_n - y_{n+1}}{y_{n-1} - y_n}\right]} \right) \tag{2}$$

$K_{\mathrm{Oy}} a_{\mathrm{m}}|_n$ is the product of the overall mass-transfer coefficient based on the vapor phase with the area involved in mass transfer per unit volume on stage "n," and HETP_n is the packed depth corresponding to theoretical plate "n." This expression can be rearranged to

$$G = (K_{\mathrm{Oy}} a_{\mathrm{m}})|_n \,\mathrm{HETP}_n \left(\frac{1 - \frac{(y_{n-1} - y_n)}{(y_n - y_{n+1})}}{\ln\left[\frac{y_n - y_{n+1}}{y_{n-1} - y_n}\right]} \right) \tag{3}$$

It can be shown that

$$\frac{y_n - y_{n+1}}{y_{n-1} - y_n} = \frac{L}{m_n G} \tag{4}$$

Substituting

$$G = (K_{\mathrm{Oy}} a_{\mathrm{m}})|_n \,\mathrm{HETP}_n \left(\frac{1 - \frac{m_n G}{L}}{\ln\left[\frac{m_n G}{L}\right]} \right) \tag{5}$$

Further, if we define $\lambda_n = m_n G/L$, then

$$\mathrm{HETP}_n = \frac{G}{(K_{\mathrm{Oy}} a)|_n} \left(\frac{\ln \lambda_n}{\lambda_n - 1} \right) \tag{6}$$

This is the final expression for the HETP at stage "n"—HETP_n. λ_n can be considered a sort of stripping factor. The notation above—HETP_n, $K_{\mathrm{Oy}} a|_n$, and λ_n—implies that these quantities are dependent on the stage number, n, whereas G is not (because of the assumption of constant molal overflow). Figure 2 shows how $\ln(\lambda)/(\lambda - 1)$ varies with λ. Clearly, the variation in the value of HETP_n can be greatly affected by λ_{n} as one moves from stage to stage. Therefore, λ has a great impact on the economics of any separation.

To calculate the packed depth required to accomplish a given level of separation, one must perform the sum shown below

$$Z = \sum_{n=1}^{N} \mathrm{HETP}_n = G \sum_{n=1}^{N} \frac{1}{(K_{\mathrm{Oy}} a_{\mathrm{m}})|_n} \left(\frac{\ln \lambda_n}{(\lambda_n - 1)} \right) \tag{7}$$

The simple appearance of this formula is deceptive. A significant amount of computational effort is required for each stage. In practice, this calculation is seldom, if ever, done.

The average HETP

The usual experimental method for measuring the efficiency of a packed section involves the calculation of a rather different HETP: the packed section, or average, HETP. This is defined as

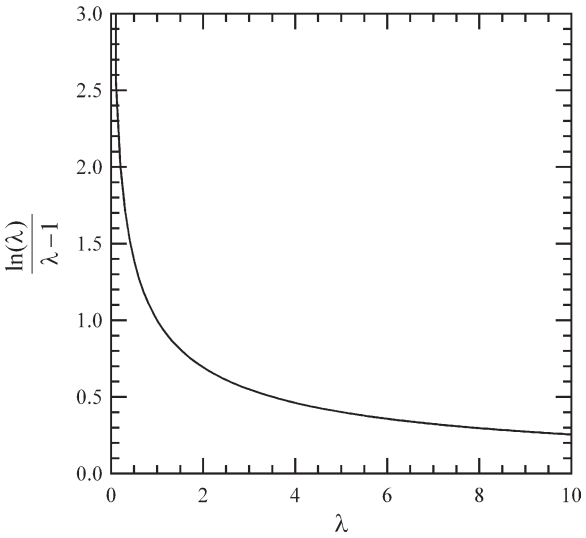

Figure 2. Factor relating the HETP to the HTU, ln(λ)/(λ − 1), as a function of λ.

$$\langle \mathrm{HETP} \rangle = \frac{Z}{N} = \frac{1}{N}\sum_{n=1}^{N} \mathrm{HETP}_n = \frac{G}{N}\sum_{n=1}^{N} \frac{1}{(K_{\mathrm{Oy}} a_{\mathrm{m}})|_n}\left(\frac{\ln \lambda_n}{(\lambda_n - 1)}\right) \quad (8)$$

The average HETP—⟨HETP⟩—has the advantage of being easy to calculate from experimental data. However, it is clearly not the same as the point HETP. The two are related in that the packed-section HETP is the average value of the individual-point HETPs.

Usually, it is the average HETP for a packed section that is reported. The variation of these average HETPs with vapor and liquid loadings, system physical properties, packing topology, and packed depth is then usually modeled with the equations developed for the point HETP. To use the point HETP equation and apply it to average HETP data, one must calculate the sum in Eq. 8. This calculation is almost never performed. Rather, the average HETP is taken to be

$$\langle \mathrm{HETP} \rangle = \frac{G}{\langle K_{\mathrm{Oy}} a_{\mathrm{m}} \rangle}\left(\frac{\ln \bar{\lambda}}{\bar{\lambda} - 1}\right) \quad (9)$$

where $\bar{\lambda}$ (= $\overline{m}$ at total reflux) is some type of average value whose value or method of calculation is rarely reported.[6,16,17] Clearly

$$\frac{\ln \bar{\lambda}}{\langle K_{\mathrm{Oy}} a_{\mathrm{m}} \rangle (\bar{\lambda} - 1)} \neq \frac{1}{N}\sum_{n=1}^{N} \frac{\ln(\lambda_n)}{(K_{\mathrm{Oy}} a_{\mathrm{m}})|_{m_n}(\lambda_n - 1)} \quad (10)$$

It is also generally true that

$$\frac{\ln \bar{\lambda}}{(\bar{\lambda} - 1)} \neq \frac{1}{N}\sum_{n=1}^{N} \frac{\ln(\lambda_n)}{(\lambda_n - 1)} \quad (11)$$

Reconciling the HETP definitions

The above description of the two different HETP definitions in use shows that the sum

$$\frac{1}{N}\sum_{n=1}^{N} \frac{\ln(\lambda_n)}{(K_{\mathrm{Oy}} a_{\mathrm{m}})|_{m_n}(\lambda_n - 1)} \quad (12)$$

must be performed to apply the point HETP definition to average HETP data usually reported. This is a challenging task. To illustrate the experimental and computational complexity implied in this sum, let us consider rectification at total reflux (i.e., $\lambda_n = \mathrm{m}_n$) of a binary pair, where the relative volatility, α, over the entire composition spectrum is constant. First, the total number of stages needs to be determined from the experimental composition data recorded at the bottom and the top of the packed section. The number of stages can be calculated with the Fenske equation:[15]

$$N = \frac{\ln\left(\frac{x_{\mathrm{t}}(1-x_{\mathrm{b}})}{x_{\mathrm{b}}(1-x_{\mathrm{t}})}\right)}{\ln(\alpha)} - 1 \quad (13)$$

Note that reboilers are usually treated as ideal stages; hence, one equilibrium stage is usually subtracted from the stage count for the entire column so that the number of stages relates only to those generated by the column internals. Next, we must enumerate the compositions at every stage. Starting at the top of the packed section, we next calculate the composition at stage 1 (numbering stages from the top down)

$$1 = \frac{\ln\left(\frac{x_{\mathrm{t}}(1-x_1)}{x_1(1-x_{\mathrm{t}})}\right)}{\ln(\alpha)} \quad (14)$$

We proceed down the column until we reach the bottom composition

$$1 = \frac{\ln\left(\frac{x_1(1-x_2)}{x_2(1-x_1)}\right)}{\ln(\alpha)} = \frac{\ln\left(\frac{x_2(1-x_3)}{x_3(1-x_2)}\right)}{\ln(\alpha)} = \cdots = \frac{\ln\left(\frac{x_{N-1}(1-x_N)}{x_N(1-x_{N-1})}\right)}{\ln(\alpha)} \quad (15)$$

The vapor mole fractions in equilibrium with the set of liquid mole fractions just enumerated can be found from

$$y^* = \frac{\alpha x}{1 + (\alpha - 1)x} \quad (16)$$

Then, the average slope of the equilibrium curve for each stage must be calculated from

$$m_n = \frac{y_n^* - y_{n-1}^*}{x_n - x_{n-1}} \quad y* = F(x, P) \quad (17)$$

Finally, the overall mass-transfer coefficient must be calculated at each stage from

$$\frac{1}{K_{\mathrm{Oy}} a_{\mathrm{m}}|_n} = \frac{1}{k_{\mathrm{y}} a_{\mathrm{m}}|_n} + \frac{m_n}{k_{\mathrm{x}} a_{\mathrm{m}}|_n} \quad (18)$$

With this, all of the information necessary to compute the necessary summation is available. Obviously, this procedure involves a great deal of calculation.

If the number of stages is large enough and the variation in the local binary relative volatility is not too severe, then a good approximation can be made to the summation in Eq. 8 by replacing it with an integral.*[18,19] If we consider a small composition change over a small increment in stage number where the relative volatility is approximately constant, then it is easy to show from the Fenske equation that†

$$\frac{dn}{dx} = \frac{1}{x(1-x)\ln[\alpha(x)]} \tag{19}$$

Equation 19 was derived assuming that the relative volatility can be considered constant during the differentiation but then replaced with the compositionally dependent α after the differentiation. Thus

$$\int_0^{N+1} dn = N+1 \cong \int_{x_b}^{x_t} \frac{dx}{x(1-x)\ln[\alpha(x)]} \tag{20}$$

or for any two stages in the column

$$\int_{n_j}^{n_1} dn = n_i - n_j \cong \int_{x_j}^{x_i} \frac{dx}{x(1-x)\ln[\alpha(x)]} \tag{21}$$

Note that the restriction of the Fenske equation to constant relative volatility has been removed.

Next, the packed-height calculation can be approximated

$$Z = \int_{N+1}^{0} \mathrm{HETP}(n)\,dn = \int_{x_b}^{x_t} \mathrm{HETP}(x)\frac{dn}{dx}dx \cong G\int_{x_b}^{x_t}\left(\frac{1}{k_y a_m} + \frac{m(x)}{k_x a_m}\right)\left(\frac{1}{x(1-x)\ln[\alpha(x)]}\right)\frac{\ln[m(x)]}{m(x)-1}dx \tag{22}$$

Thus

$$\langle \mathrm{HETP}\rangle = \frac{Z}{N} \cong G\frac{\int_{x_b}^{x_t}\left(\frac{1}{k_y a_m}\right)\left(\frac{1}{x(1-x)\ln[\alpha(x)]}\right)\frac{\ln[m(x)]}{m(x)-1}dx}{\int_{x_b}^{x_t}\frac{dx}{x(1-x)\ln[\alpha(x)]}} + G\frac{\int_{x_b}^{x_t}\left(\frac{1}{k_x a_m}\right)\left(\frac{m(x)}{x(1-x)\ln[\alpha(x)]}\right)\frac{\ln[m(x)]}{m(x)-1}dx}{\int_{x_b}^{x_t}\frac{dx}{x(1-x)\ln[\alpha(x)]}} \tag{23}$$

where‡

$$m(x) = \frac{\alpha(x)}{(1+[\alpha(x)-1]x)^2} \tag{24}$$

*It is less disturbing to do this with a packed column where it is easier to imagine the composition being continuous with packed depth.

†See Appendix A.

‡We have ignored terms involving $d\alpha/dx$ in the derivation of Eq. 24 from Eq. 16. For the standard distillation systems studied in most laboratories, the variation of the relative volatility with composition is small, and the neglect of these terms has negligible impact. See Appendix B.

Let us now assume that the terms $k_y a$ and $k_x a$ vary only slightly over the length of bed in question and that they can be withdrawn from their respective integrals and replaced by an average value for the length of bed in question. Then

$$\langle \mathrm{HETP}\rangle = \frac{Z}{N} = G\left(\frac{C_y}{k_y a_m} + \frac{C_x}{k_x a_m}\right) \tag{25}$$

where

$$C_y = \frac{\int_{x_b}^{x_t}\left(\frac{1}{x(1-x)\ln[\alpha(x)]}\right)\frac{\ln[m(x)]}{m(x)-1}dx}{\int_{x_b}^{x_t}\frac{dx}{x(1-x)\ln[\alpha(x)]}} = \left\langle \frac{\ln[m(x)]}{m(x)-1}\right\rangle \tag{26}$$

$$C_x = \frac{\int_{x_b}^{x_t}\left(\frac{m(x)}{x(1-x)\ln[\alpha(x)]}\right)\frac{\ln[m(x)]}{m(x)-1}dx}{\int_{x_b}^{x_t}\frac{dx}{x(1-x)\ln[\alpha(x)]}} = \left\langle \frac{m(x)\ln[m(x)]}{m(x)-1}\right\rangle \tag{27}$$

$$\langle \mathrm{HETP}\rangle = \frac{Z}{N} = \frac{G}{a_m}\left(\frac{C_y}{k_y} + \frac{C_x}{k_x}\right) \tag{28}$$

Although the calculations look overwhelming, they are actually quite easy to perform numerically—in fact, these integrals are substantially easier to evaluate than the sums discussed earlier. Further, there is no restriction on these equations to constant relative volatility.

Even without evaluating these integrals some important conclusions can be drawn. First, note that $\langle \mathrm{HETP}\rangle$ now depends explicitly on the bottom and top compositions. So, it is not enough to just report $\langle \mathrm{HETP}\rangle$, one must also report the top and bottom compositions as well. Second, as the bottom and top compositions depend on the packed depth, we should expect to see that $\langle \mathrm{HETP}\rangle$ is packed depth dependent. Indeed, this is oftentimes observed,[20–22] and the effect is sometimes even included in packed-column mass-transfer correlations.[4,23,24] Figure 3 shows how C_y and C_x vary with the mole fraction of the light component for a fictitious binary mixture with $\alpha = 1.2$ and the bottom composition fixed at $x_b = 0.05$.

Dimensional analysis

First, we consider expressions for the mass-transfer coefficients

$$k_y = K_y(v_V, \rho_V, \mu_V, c_V, D_V, d_e) \tag{29}$$

$$k_x = K_x(v_L, \rho_L, \mu_L, c_L, D_L, d_e) \tag{30}$$

In each case, we have assumed that there are seven quantities with physical dimensions. Further, we note that there are four units of dimension in the relationships above (mass, length, time, and mole number). By the Buckingham Π theorem, a relationship exists among three dimensionless groupings.[25] It is straightforward to show in each case that the Sherwood number can be taken to depend on the Reynolds number and the Schmidt number.

$$Sh_V = \frac{k_y d_e}{c_V D_V} = A_V Re_V^m Sc_V^n \tag{31}$$

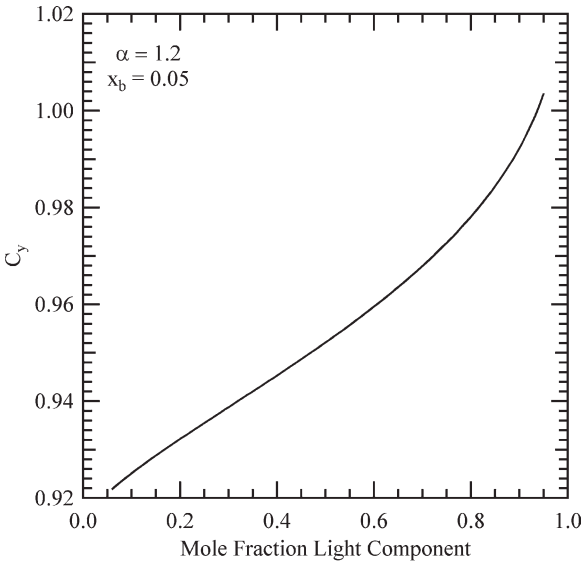

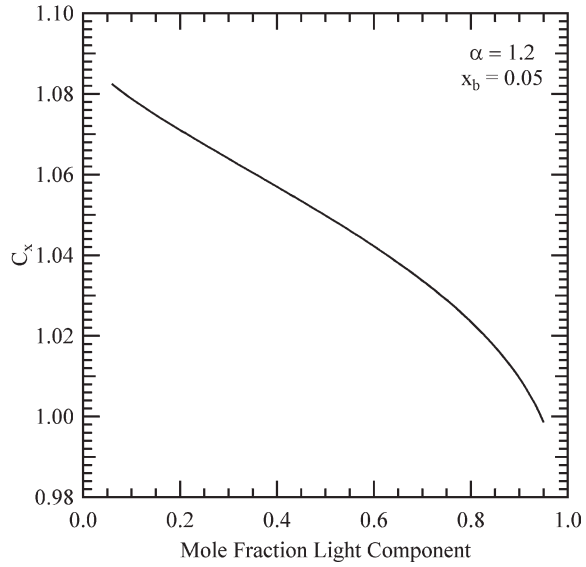

Figure 3. Vapor-side and liquid-side composition correction factors appearing in Eq. 25 for ⟨HETP⟩.

$$Sh_L = \frac{k_x d_e}{c_L D_L} = A_L Re_L^b Sc_L^c \tag{32}$$

These are the expressions for the mass-transfer coefficients that we will use.

Next, consider the fractional mass-transfer area, a_m/a_d. Let us assume that the fractional mass-transfer area in a packed tower is a function of the following physical quantities

$$\frac{a_m}{a_d} = F(\rho_V, \mu_V, v_V, \rho_L, \mu_L, v_L, \sigma, d_e, g)$$
$$\rho \to \frac{m}{l^3} \quad \mu \to \frac{m}{l-t} \quad \sigma \to \frac{m}{t^2} \quad v \to \frac{l}{t} \quad d_e \to l \quad g \to \frac{l}{t^2} \tag{33}$$

Because there are nine quantities with physical dimensions and three units of dimension (mass, length, and time), the fractional mass-transfer area will be a function of six dimensionless groupings. In one method for finding the dimensionless groupings, we assume that the functional form for a_m/a_d is a power law. Doing so allows us to write down a set of linear equations relating the power-law exponents on the various physical quantities.

$$\frac{a_m}{a_d} \propto (\rho_V)^\alpha (\mu_V)^\beta (v_V)^\chi (\rho_L)^\delta (\mu_L)^\varepsilon (v_L)^\phi (\sigma)^\gamma (d_e)^\eta (g)^\iota \tag{34}$$

$$m^0 l^0 t^0 = \left(\frac{m}{l^3}\right)^\alpha \left(\frac{m}{l-t}\right)^\beta \left(\frac{l}{t}\right)^\chi \left(\frac{m}{l^3}\right)^\delta \left(\frac{m}{l-t}\right)^\varepsilon \left(\frac{l}{t}\right)^\phi \left(\frac{m}{t^2}\right)^\gamma (l)^\eta \left(\frac{l}{t^2}\right)^\iota \tag{35}$$

Thus

$$\begin{aligned} 0 &= \alpha + \beta + \delta + \varepsilon + \gamma && \text{(mass)} \\ 0 &= -3\alpha - \beta + \chi - 3\delta - \varepsilon + \phi + \eta + \iota && \text{(length)} \\ 0 &= -\beta - \chi - \varepsilon - \phi - 2\gamma - 2\iota && \text{(time)} \end{aligned} \tag{36}$$

Some manipulation allows us to express γ, η, and ι in terms of α, β, χ, δ, ε, and ϕ.

$$\begin{aligned} \gamma &= -\alpha - \beta - \delta - \varepsilon \\ \eta &= 2\alpha + \beta/2 - \chi/2 + 2\delta + \varepsilon/2 - \phi/2 \\ \iota &= \alpha + \beta/2 - \chi/2 + \delta + \varepsilon/2 - \phi/2 \end{aligned} \tag{37}$$

Substituting

$$\frac{a_m}{a_d} \propto (\rho_V^\alpha)(\mu_V^\beta)(v_V^\chi)(\rho_L^\delta)(\mu_L^\varepsilon)(v_L^\phi)(\sigma^{-\alpha-\beta-\delta-\varepsilon}) \times (d_e^{2\alpha+\beta/2-\chi/2+2\delta+\varepsilon/2-\phi/2})(g^{\alpha+\beta/2-\chi/2+\delta+\varepsilon/2-\phi/2}) \tag{38}$$

and then collecting terms with the same power-law exponents gives us the following

$$\frac{a_m}{a_d} \propto \left(\frac{\rho_V d_e^2 g}{\sigma}\right)^\alpha \left(\frac{\mu_V d_e^{1/2} g^{1/2}}{\sigma}\right)^\beta \left(\frac{v_V}{d_e^{1/2} g^{1/2}}\right)^\chi \left(\frac{\rho_L d_e^2 g}{\sigma}\right)^\delta \times \left(\frac{\mu_L d_e^{1/2} g^{1/2}}{\sigma}\right)^\varepsilon \left(\frac{v_L}{d_e^{1/2} g^{1/2}}\right)^\phi \tag{39}$$

or

$$\frac{a_m}{a_d} \propto (Bo_V)^\alpha \left(\frac{\mu_V d_e^{1/2} g^{1/2}}{\sigma}\right)^\beta \left(\sqrt{Fr_V}\right)^\chi (Bo_L)^\delta \times \left(\frac{\mu_L d_e^{1/2} g^{1/2}}{\sigma}\right)^\varepsilon \left(\sqrt{Fr_L}\right)^\phi \tag{40}$$

These dimensionless groupings are less well known than the Reynolds number, Weber number, and Froude number

$$Re_V = \frac{d_e v_V \rho_V}{\mu_V} \quad Re_L = \frac{d_e v_L \rho_L}{\mu_L}$$
$$We_L = \frac{d_e \rho_L v_L^2}{\sigma} \quad Fr_L = \frac{v_L^2}{g d_e}$$

After some substitutions, we arrive at the following alternate relationship for a_m/a_d

$$\frac{a_m}{a_d} \propto \left(\frac{\rho_V}{\rho_L}\right)^{\alpha-\chi}\left(\frac{\mu_V}{\mu_L}\right)^{\beta+\chi}(Re_L^{-\beta-\chi-\varepsilon})(Fr_L^{\phi/2-\alpha-\beta/2+\chi/2-\varepsilon/2}) \times (We_L^{\alpha+\beta+\varepsilon})(Re_V^{\chi}) \quad (41)$$

Our final equation for a_m/a_d is

$$\frac{a_m}{a_d} = A_M\left(\frac{\rho_V}{\rho_L}\right)^{A}\left(\frac{\mu_V}{\mu_L}\right)^{B}(Re_L^X)(Fr_L^\Delta)(We_L^E)(Re_V^\Phi) \quad (42)$$

Note the appearance of the groups (ρ_V/ρ_L) and (μ_V/μ_L) in our equation for a_m/a_d. These groups have either not been considered in the development of other correlations for the mass-transfer area or the exponents A and B have been assumed to be zero a priori.[3–5] We choose to retain these two groups.

For sheet metal structured packings, we adjust Eq. 42 in an ad hoc way to allow it to account for the corrugation inclination angle

$$\frac{a_m}{a_d} = A_M\left(\frac{\rho_V}{\rho_L}\right)^{A}\left(\frac{\mu_V}{\mu_L}\right)^{B}(Re_L^X)(Fr_L^\Delta)(We_L^E)(Re_V^\Phi)\left(\frac{\cos(\theta)}{\cos(\pi/4)}\right)^{t} \quad (43)$$

where "θ" is the corrugation inclination angle in radians measured from the vertical. The adjustment for correlation inclination angle in Eq. 43 allows us to develop a single set of fitting coefficients for all inclination angles rather than developing individual correlating expressions for each inclination angle.

Final expression for the ⟨HETP⟩

Substituting rearranged versions of Eqs. 31, 32, and 42 into Eq. 28 for ⟨HETP⟩ yields (for random packings and metal gauze "X" style packings; a further adjustment for corrugation inclination angle appears in the general formulation for sheet metal structured packings, as discussed above)

$$\langle \mathrm{HETP}\rangle = \frac{Gd_e}{\left(A_M\left(\frac{\rho_V}{\rho_L}\right)^{A}\left(\frac{\mu_V}{\mu_L}\right)^{B}(Re_L^X)(Fr_L^\Delta)(We_L^E)(Re_V^\Phi)a_d\right)} \times \left(\frac{C_y}{A_V Re_V^m Sc_V^n c_V D_V} + \frac{C_x}{A_L Re_L^b Sc_L^c c_L D_L}\right) \quad (44)$$

We immediately see that the Eq. 44 for the ⟨HETP⟩ expressed in terms of independent expressions for k_y, k_x, and a_m (opposed to expressions for the combined quantities $k_y a_m$ and $k_x a_m$) is not unique. It is possible to factor out the front factor A_L (for example) and define two new relative front factors for k_y and a_m

$$\langle \mathrm{HETP}\rangle = \frac{Gd_e}{\left(A'_M\left(\frac{\rho_V}{\rho_L}\right)^{A}\left(\frac{\mu_V}{\mu_L}\right)^{B}(Re_L^X)(Fr_L^\Delta)(We_L^E)(Re_V^\Phi)a_d\right)} \times \left(\frac{C_y}{A'_V Re_V^m Sc_V^n c_V D_V} + \frac{C_x}{Re_L^b Sc_L^c c_L D_L}\right) \quad (45)$$

where

$$A'_M = A_M A_L \quad (46)$$

$$A'_V = A_V/A_L \quad (47)$$

Therefore, it is not generally possible to deconvolute experimentally measured ⟨HETP⟩ data from binary distillation experiments into unique correlating expressions for k_y, k_x, and a_m from the ⟨HETP⟩ dataset alone. To resolve the "Eq. 45" dilemma, the absolute magnitude of any one of the front factors—A_V, A_L, and A_M—appearing in Eq. 44 must be established.

Equation 44 contains 13 fitting coefficients. Ten of these appear as exponents on dimensionless groupings. Trying to fit data to an equation in which the same physical quantity simultaneously contributes to one or more dimensionless groups in the equation presents statistical difficulties.[26] Meaningless correlations have been known to result when variations in the data to be fit and in the physical parameters making up the dimensionless groupings are sufficiently large and random.[27]

To try to avoid the majority of these statistical difficulties, we shall fix the values of several of the power-law exponents in Eq. 44 by appealing to verified results from other types of experiments or to some type of mechanistic/heuristic analogy between fluid friction and mass transfer.

The mass-transfer coefficient correlation for vapor flow

Churchill[28] presented a detailed discussion of several of the gas-side mass-transfer correlations derived from classical hydraulic analogies. One such analogy is that of Chilton and Colburn[29]

$$j_D = \frac{Sh_V}{Re_V^1 Sc_V^{1/3}} = \frac{f}{2} \quad (48)$$

$$f = F(Re_V) \quad (49)$$

where "f" is the friction factor. Although the correlation is at odds with some theoretical findings, it is reasonably accurate for flows in which no form drag is present. The packings we are considering here—metal Pall rings, metal IMTP, and sheet metal structured packings with crimp geometries similar MELLAPAK—have open structures; therefore, form drag should be small. Rather than using the Chilton–Colburn analogy in its "strong" form, we shall instead use a "weak" form of Eq. 48

$$j_D \propto J_D(Re_V) \quad (50)$$

For vapor flow through Pall rings, IMTP, and sheet metal structured packings, the dry friction factor is often found to be weakly dependent on the Reynolds number (often $f \propto Re_V^{-0.2\ \mathrm{to}\ 0}$). Therefore, we assume that the vapor-phase Sherwood number scales like

$$Sh_V \propto Re_V^1 Sc_V^{1/3} \quad (51)$$

for random packings. There is an additional effect of corrugation inclination angle on the vapor-side mass-transfer coefficient for sheet metal structured packings. For these, we assume

$$Sh_V \propto Re_V^1 Sc_V^{1/3} \left(\frac{\cos(\theta)}{\cos(\pi/4)}\right)^s \quad (52)$$

where "θ" is the corrugation inclination angle in radians measured from the vertical. The metal gauze "X" style structured packings (BX, DX, and EX) tend to have smaller flow channels with friction factors that are more strongly dependent on the vapor Reynolds number. For them, we assume

$$Sh_V \propto Re_V^{1/2} Sc_V^{1/3} \quad (53)$$

The mass-transfer coefficient correlation for liquid film flow

Mathematical solution of the hydrodynamic and mass conservation equations for the absorption of a slightly soluble gas into a laminar, falling, liquid film on a plane surface gives the following result for the liquid-side mass-transfer coefficient[30]

$$Sh_L = 1.128 Re_L^{1/2} Sc_L^{1/2} \quad (54)$$

However, the liquid film's flow regime in most packed columns is expected to be turbulent, partly due to the induced shear at the liquid interface due to the turbulent countercurrent flow of the vapor. There is much less general consensus for the form of the liquid-film mass-transfer coefficient relation under these circumstances. Two models often chosen to describe mass transfer in a turbulent liquid film are the penetration/surface renewal model and the film model.[31,32] The film model predicts that the liquid-side mass-transfer coefficient is directly proportional to the binary diffusivity. This implies that

$$Sh_L \propto Sc_L^0 \quad (55)$$

Penetration/surface renewal theory, on the other hand, predicts that the liquid-side mass-transfer coefficient is proportional to the square root of the liquid diffusivity, so that

$$Sh_L \propto Re_L^1 Sc_L^{1/2} f(Re_L) \quad (56)$$

Assuming that the friction factor is nearly independent of Reynolds number, Eq. 56 reduces to

$$Sh_L \propto Re_L^1 Sc_L^{1/2} \quad (57)$$

Turning now to the experiment, Sherwood and Holloway[33] correlated absorption and desorption data for various gases in water with the expression

$$Sh_L = \alpha \left(\frac{L}{\mu_L}\right)^{1-n} Sc_L^{1/2} \quad (58)$$

with the exponent "n" ranging from 0.22 to 0.46 for Raschig rings and saddles. Koch et al.[34] measured liquid-film mass-transfer coefficients for the absorption of CO_2 into water using Raschig rings and found

$$k_L a_m \propto L^{0.96} \quad (59)$$

Van Krevelen and Hoftijzer[35] postulated that

$$\frac{k_L \delta}{D_L} = c' Re_L^b Sc_L^{1/3} \quad (60)$$

Potnis and Lenz[36] studied liquid desiccant systems for gas drying using random as well as structured packings. They reported that

$$Sh_L \propto Re_L^b Sc_L^{1/2} \quad (61)$$

with the exponent "b" ranging from 0.9 to 1.2. Shetty and Cerro[37] studied the flow of liquid films over periodic surfaces similar to those found in structured packings. They predicted that

$$Sh_L \propto Re_L^{1/3} Sc_L^{1/2} \quad (62)$$

Given the wide variability in the values of the power-law exponents on the liquid Reynolds number and Schmidt number, we have assumed that

$$Sh_L = A_L Re_L^1 Sc_L^{1/3} \quad (63)$$

holds for metal Pall rings, metal IMTP, sheet metal structured packings, and metal gauze structured packings. Equation 63 can be taken to imply that a form of the Chilton–Colburn analogy holds for turbulent liquid film flow.

Analysis Methodology

The variation of the $\langle$HETP$\rangle$ with liquid and vapor flow rates can be quite complex. Figure 4 is an illustration of "typical" $\langle$HETP$\rangle$ behavior for a binary distillation at total reflux. For low liquid rates, there is a deterioration in column efficiency due to underwetting of the packing. The efficiency also deteriorates near flood. Sometimes, there is also a region near loading with enhanced column efficiency.[38] The simple power-law expressions that we have proposed for k_y, k_x, and a_m cannot reproduce the complexity of this typical $\langle$HETP$\rangle$ behavior. Therefore, we have limited our analysis to the intermediate regions of the $\langle$HETP$\rangle$ function, where the variations of the $\langle$HETP$\rangle$ with flow rate are more amenable to description with simple power-law expressions for k_y, k_x, and a_m.

Because the contribution of the liquid-side resistance has been found to be small in the great majority of binary distillations, we will proceed by setting the front factor, A_L, in Eq. 44 to unity (this is equivalent to using Eq. 45). This then fixes the contribution of the small liquid-side resistance to the $\langle$HETP$\rangle$. As the small contribution of the liquid-phase resistance is now completely specified, we can curve fit experimental $\langle$HETP$\rangle$ data to Eq. 45 to determine the power-law exponents on the various dimensionless groups and to

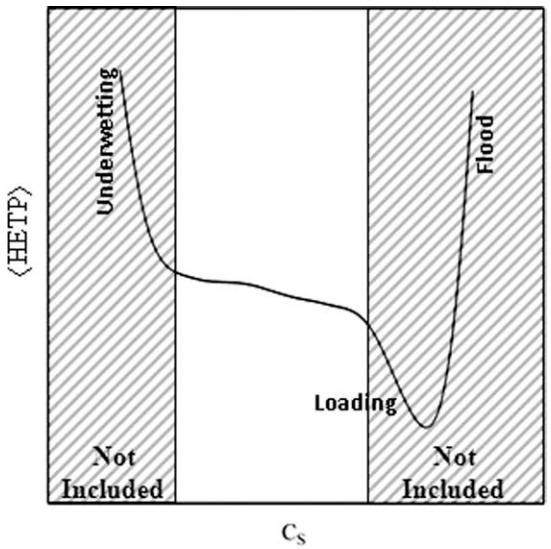

Figure 4. Schematic showing the potentially complicated variation of ⟨HETP⟩ with density-corrected vapor flow, C_S, for a column operating at total reflux.

Data from the regions labeled "not included" were not included in datasets used in the regressions described in the text.

obtain the relative values of the front factors A'_M ($= A_M A_L$) and A'_V ($= A_V/A_L$).

Once this curve fit has been performed, then determining the absolute values of the front factors A_L, A_V, and A_M proceeds by analyzing a different experiment or set of experiments where the contribution of the individual phase resistances to the overall resistance is different. Typically, we have accomplished this by looking at CO_2 absorption into aqueous amine or aqueous caustic solutions. We use the mass-transfer correlations regressed from the binary distillation experiments to predict the performance of the CO_2 absorber (and sometimes the stripper) using the *Aspen Rate Based Distillation* module.[2] Initially, the front factors values are fixed at $A_L = 1$, A'_V, and A'_M. The predicted temperature profile, outlet CO_2 concentration, and outlet amine loading are noted, and their deviation from experiment recorded. If necessary, the front factor A_L is adjusted to some new value, keeping A'_V and A'_M fixed. The reader should recall that $A'_M = A_L A_M$ and that $A'_V = A_V/A_L$. We typically use an interval halving method to determine the best value for A_L. There is some judgment involved in deciding what value for A_L is best overall as the analysis of individual experiments oftentimes leads to a spread in A_L values. A flow diagram outlining the fitting process to identify A_L, A_M, and A_V is shown in Figure 5.

Data Sources and Data Correlation

⟨HETP⟩ data for binary distillation systems and temperature profile/amine loading/outlet sour gas composition data from acid gas absorption/stripping experiments were collected for the packing types under study here.[9–12,20–22,39–63]

The data for the various packing families were individually analyzed using the methodology outlined above. Several ad hoc limiting conditions were placed upon the power-law exponents in the fits. For all but the BX style gauze structured packing power-law exponents were limited to the range −0.2 to 0.2. In the case of BX, the range was expanded to be −0.25 to 0.25. The reasons for limiting the ranges of the power-law coefficients are difficult to elucidate. Part of the explanation lies in the fact that data fitting becomes more problematic when the same physical quantity appears in more than one dimensionless grouping.[26] For example, fitting the data with no imposed restrictions would often lead power-law exponents with large magnitudes but whose net effect on some variable, usually the liquid velocity, would be small to negligible. A further consideration was the fact that many other reported mass-transfer correlations have power-law exponents on dimensionless groupings whose magnitudes are less than 1.[64] The final reason was a pragmatic one—limiting the range on these coefficients resulted in correlations whose predictions were generally better in every situation, and which turned out to be more robust in the simulator.

Metal pall rings

$$k_x = 1.0 Re_L^1 Sc_L^{1/3} \left(\frac{c_L D_L}{d_e}\right) \tag{64}$$

$$k_y = 0.00104 Re_V^1 Sc_V^{1/3} \left(\frac{c_V D_V}{d_e}\right) \tag{65}$$

$$\frac{a_m}{a_d} = 0.25 Re_V^{0.134} Re_L^{0.205} We_L^{0.075} Fr_L^{-0.164} \left(\frac{\rho_V}{\rho_L}\right)^{-0.154} \left(\frac{\mu_V}{\mu_L}\right)^{0.195} \tag{66}$$

$$\langle HETP \rangle = \frac{G d_e}{\left(A'_M \left(\frac{\rho_V}{\rho_L}\right)^A \left(\frac{\mu_V}{\mu_L}\right)^B (Re_L^X)(Fr_L^A)(We_L^B)(Re_V^\Phi) a_d\right)} \left(\frac{C_y}{A'_V Re_V^\Delta Sc_V^\Delta c_V D_V} + \frac{C_x}{Re_L^\Delta Sc_L^\Delta c_L D_L}\right)$$

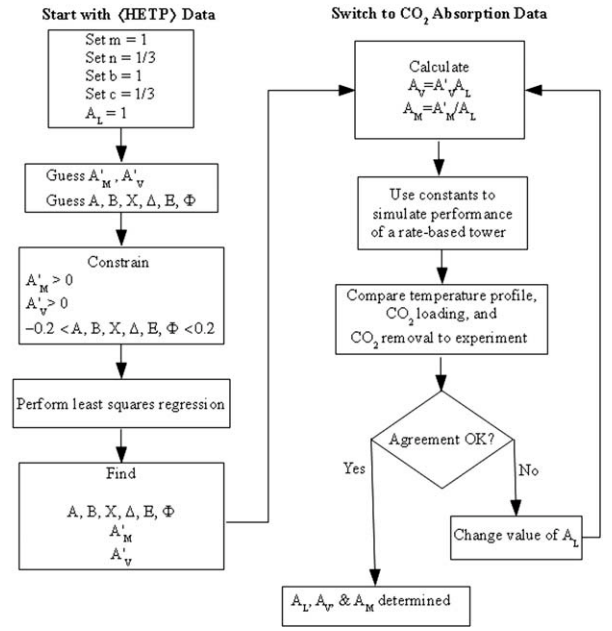

Figure 5. Diagram showing the workflow for the data fitting procedure proposed in this article.

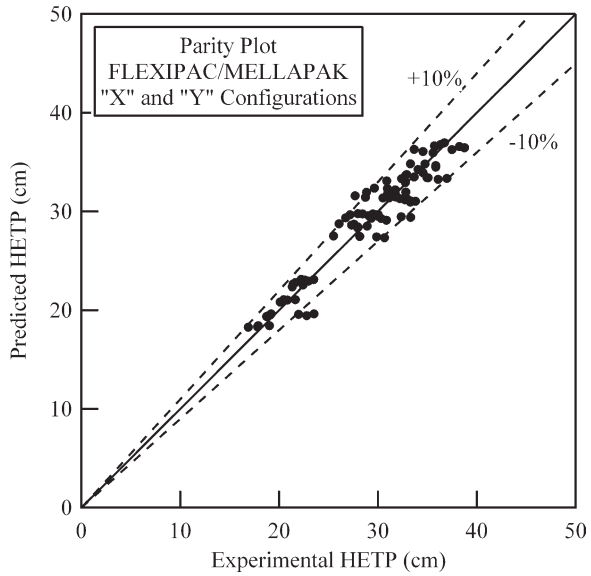

Figure 6. Parity plot comparing the calculated ⟨HETP⟩ to the experimentally measured ⟨HETP⟩ for sheet metal structured packings of the MELLAPAK/FLEXIPAC type.

Data for both the "Y" and "X" packing configurations were used in the regression.

Metal IMTP

$$k_x = 1.0 Re_L^1 Sc_L^{1/3} \left(\frac{c_L D_L}{d_e}\right) \tag{67}$$

$$k_y = 0.00473 Re_V^1 Sc_V^{1/3} \left(\frac{c_V D_V}{d_e}\right) \tag{68}$$

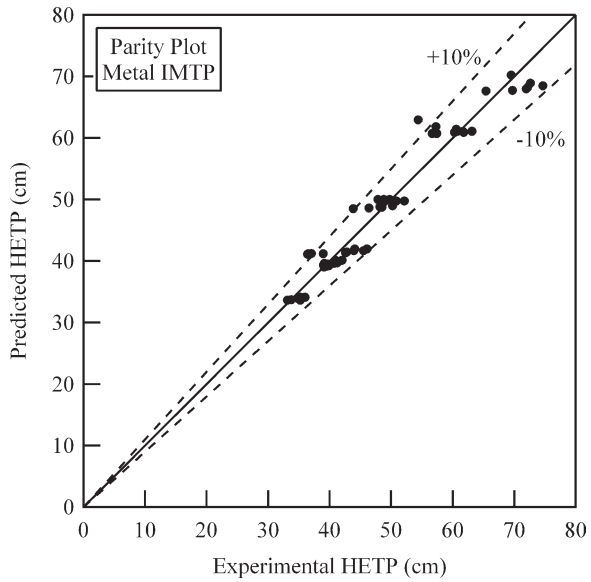

Figure 7. Parity plot comparing the calculated ⟨HETP⟩ to the experimentally measured ⟨HETP⟩ for metal IMTP random packing.

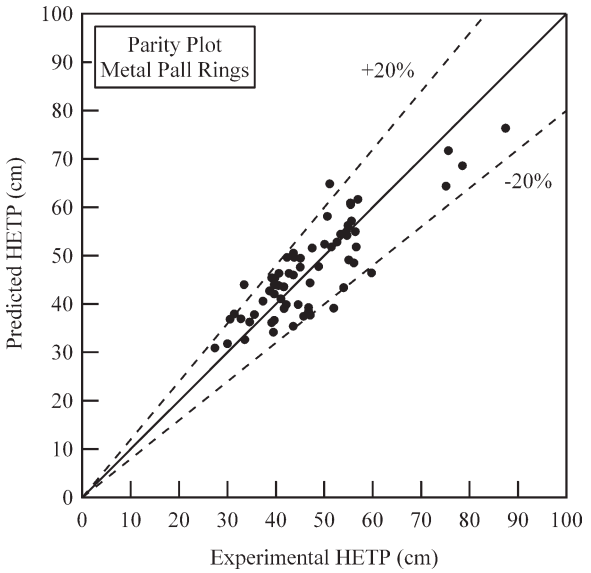

Figure 8. Parity plot comparing the calculated ⟨HETP⟩ to the experimentally measured ⟨HETP⟩ for metal Pall rings random packing.

$$\frac{a_m}{a_d} = 0.332 Re_V^{0.132} Re_L^{-0.102} We_L^{0.194} Fr_L^{-0.2} \left(\frac{\rho_V}{\rho_L}\right)^{-0.154} \left(\frac{\mu_v}{\mu_L}\right)^{0.195} \tag{69}$$

Sheet metal structured packing

$$k_x = 0.33 Re_L^1 Sc_L^{1/3} \left(\frac{c_L D_L}{d_e}\right) \tag{70}$$

$$k_y = 0.0084 Re_V^1 Sc_V^{1/3} \left(\frac{c_V D_V}{d_e}\right) \left(\frac{\cos(\theta)}{\cos(\pi/4)}\right)^{-7.15} \tag{71}$$

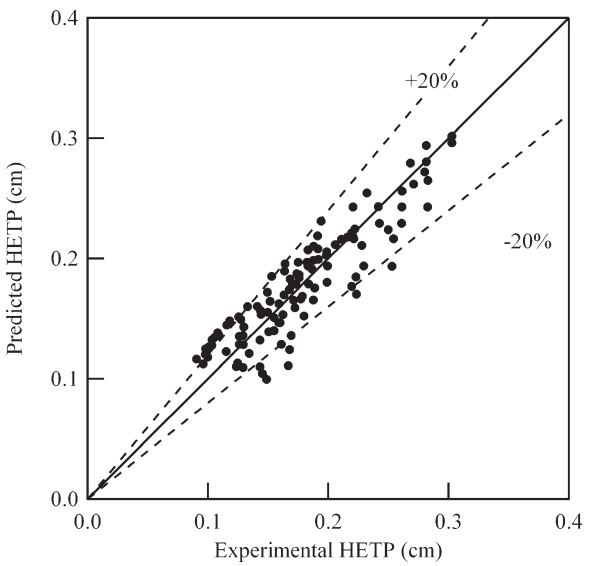

Figure 9. Parity plot comparing the calculated ⟨HETP⟩ to the experimentally measured ⟨HETP⟩ for metal gauze structured packings in the X configuration (BX, DX, and EX).

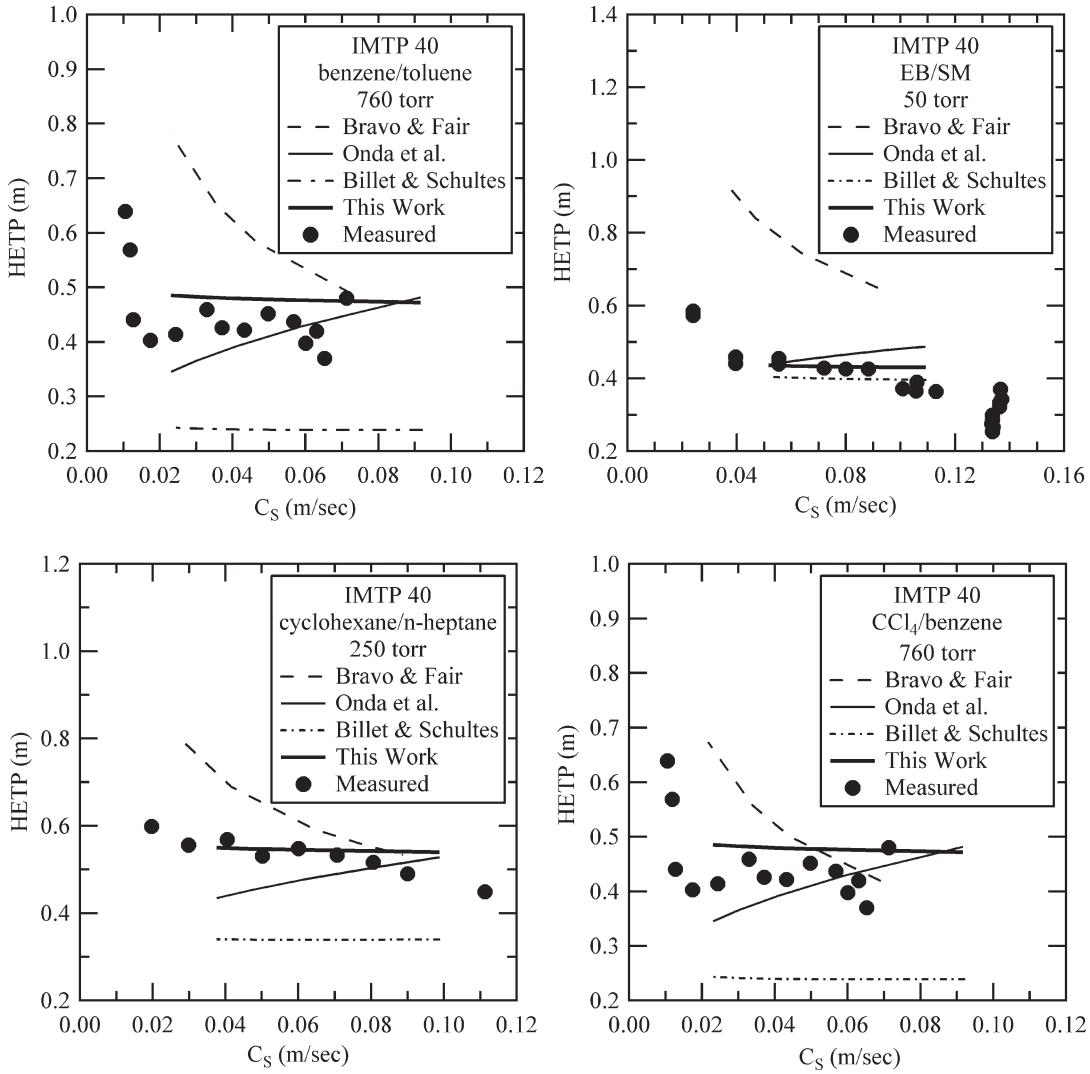

Figure 10. Comparison of correlation predictions with experimental data for metal IMTP.

(a) Data of Wang et al.[55] for total reflux distillation of benzene/toluene at 760 torr. (b) Performance data for IMTP 40 random packing in ethylbenzene/styrene service.[56] (c) Data of Wagner et al.[43] for total reflux distillation of cyclohexane/*n*-heptane at 250 torr. (d) Data of Wang et al.[55] for total reflux distillation of carbon tetrachloride/benzene at 760 torr. Correlations used in these calculations: Bravo and Fair,[4] Onda et al.,[3] and Billet and Schultes.[5]

$$\frac{a_m}{a_d} = 0.539 Re_V^{0.145} Re_L^{-0.153} We_L^{0.2} Fr_L^{-0.2} \left(\frac{\rho_V}{\rho_L}\right)^{-0.033} \left(\frac{\mu_V}{\mu_L}\right)^{0.090} \left(\frac{\cos(\theta)}{\cos(\pi/4)}\right)^{4.078} \quad (72)$$

Metal gauze structured packing in the "X" configuration

$$k_x = 12 Re_L^1 Sc_L^{1/3} \left(\frac{c_L D_L}{d_e}\right) \quad (73)$$

$$k_y = 0.3516 Re_V^{1/2} Sc_V^{1/3} \left(\frac{c_V D_V}{d_e}\right) \quad (74)$$

$$\frac{a_m}{a_d} = 2.308 Re_V^{-0.274} Re_L^{0.246} We_L^{0.248} Fr_L^{-0.161} \left(\frac{\rho_V}{\rho_L}\right)^{-0.180} \left(\frac{\mu_V}{\mu_L}\right)^{0.233} \quad (75)$$

Figure 6 is a parity plot of the predicted values for $\langle HETP \rangle$ vs. the reported values for the various MELLAPAK/FLEXIPAC family of sheet metal structured packings. Figure 7 is a similar plot for metal IMTP random packing; Figure 8 for metal Pall rings; and Figure 9 for metal gauze BX structured packing. A discussion of some further issues related to curve fitting is presented in Appendix C.

Comparison to Experiment

In this section, we compare predictions made with the mass-transfer correlations developed above to experiment for a number of different chemical systems, packing types. All calculations were carried out with *Aspen Rate Based Distillation* v7.2.[2] In general, we used the COUNTERCURRENT flow option and the NRTL physical property package for binary distillation simulations. For acid gas removal with amines or with caustic, we used the VPLUG flow option (this option

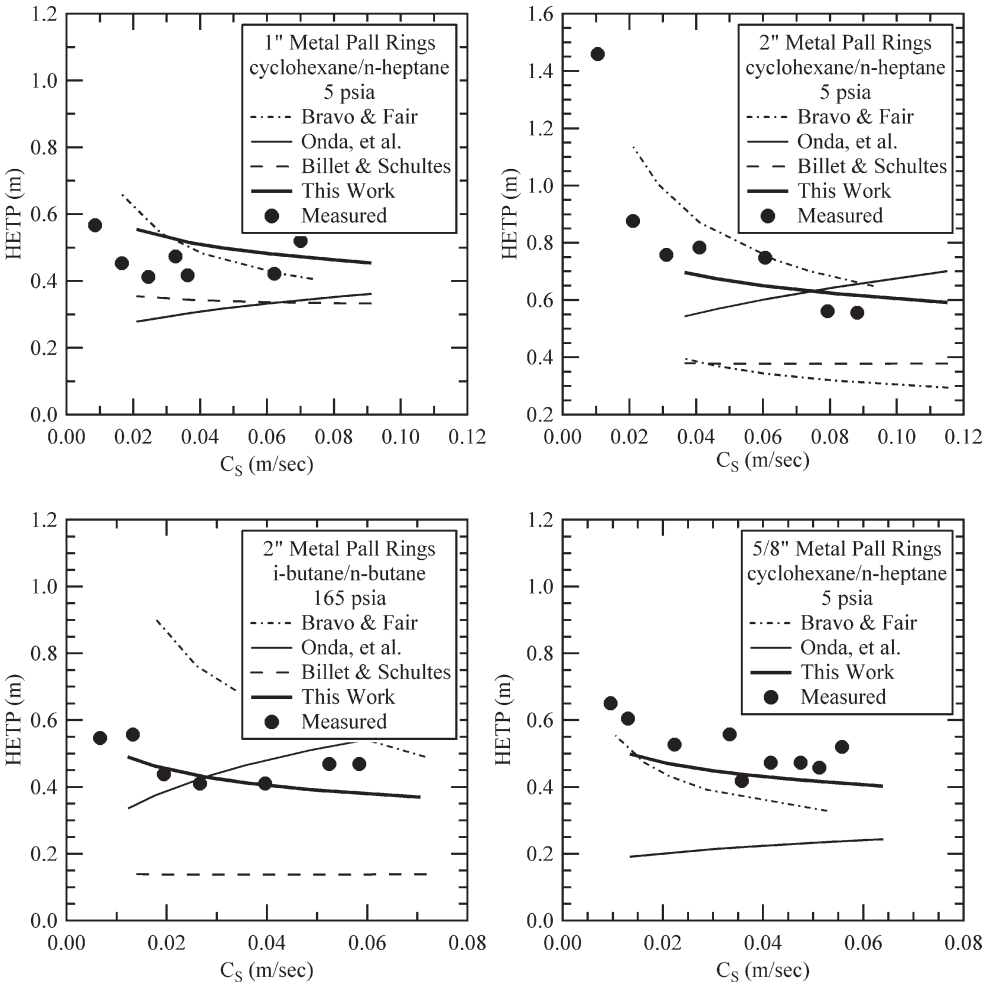

Figure 11. Comparison of correlation predictions with experimental data for metal Pall rings.

(a) Data of Shariat and Kunesh[57] for total reflux distillation of cyclohexane/*n*-heptane at 5 psia. (b) Data of Shariat and Kunesh[57] for total reflux distillation of cyclohexane/*n*-heptane at 5 psia. (c) Data from Schultes[9] for total reflux distillation of *i*-butane/*n*-butane at 165 psia. (d) Data of Shariat and Kunesh[57] for total reflux distillation of cyclohexane/*n*-heptane at 5 psia. Correlations used in these calculations: Bravo and Fair,[4] Onda et al.,[3] and Billet and Schultes.[5]

treats the liquid phase as well mixed and the vapor as in plug flow) and the ELECNRTL package for physical properties. The reader is informed wherever we have deviated from these conventions. The bases of the NRTL[65] and ELECNRTL[66] property options are described elsewhere.

Figure 10 is a comparison of total reflux binary ⟨HETP⟩ data for metal IMTP with simulated results for a selection of different binary mixtures and packing sizes. In each case, the mass-transfer coefficient correlation developed in this article for metal IMTP outperforms the other mass-transfer correlations examined.

Figure 11 is a comparison of total reflux binary ⟨HETP⟩ data for metal Pall rings with simulated results for a selection of different binary mixtures and packing sizes. In each case, the mass-transfer coefficient correlation developed in this article for metal Pall rings outperforms the other mass-transfer correlations examined.

Figure 12 is a comparison of total reflux binary ⟨HETP⟩ data for sheet metal structured packings with simulated results obtained for a selection of different binary mixtures and packing sizes. In each case, the mass-transfer coefficient correlation developed in this article for structured packings performs as well or better than the other mass-transfer correlations examined.

Tables 1 and 2 contain an additional column with ⟨HETP⟩ predictions from the new mass-transfer coefficient/interfacial-area correlations developed in this article. Clearly, the new mass-transfer/interfacial-area correlations are an improvement over the other public-domain correlations examined here across a varied range of chemical systems and packing sizes/geometries.

Lawal et al.[40] have compared pilot plant data with the results of simulation studies on the absorption of CO_2 by monoethanolamine (MEA) in a column packed with IMTP 40 metal random packing. The pilot plant data were taken by the Separations Research Program at the University of Texas, Austin.[68] Lawal et al. reported detailed results for two cases, referred to as "Case 32" and "Case 47." Case 32 is more interesting to study because the results are strongly dependent upon the mass-transfer correlation selection. In our simulations, we have used the Aspen v7.0 MEA

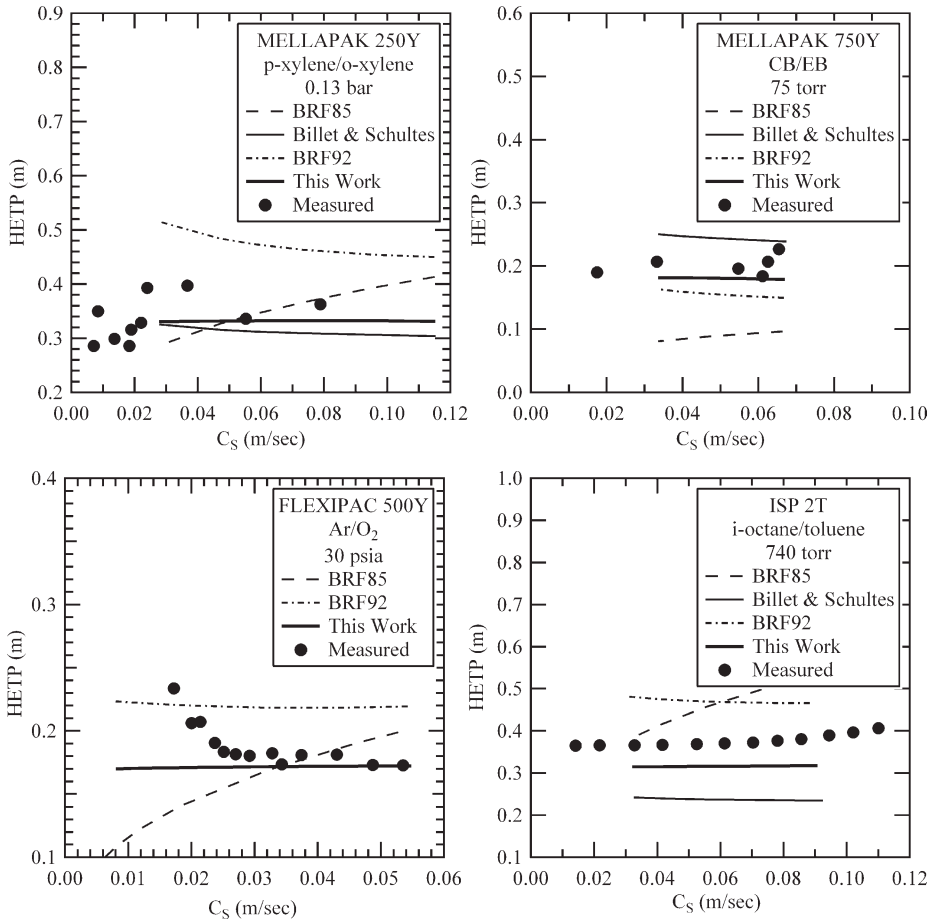

Figure 12. Comparison of correlation predictions with experimental data for sheet metal structured packings.

(a) Data of Fitz et al.[10] for total reflux distillation of cyclohexane/*n*-heptane at 5 psia. Simulations performed with the NRTL property package. (b) Data reported by Bennett and Pilling[58] for total reflux distillation of chlorobenzene/ethylbenzene at 75 torr. Simulations performed with the NRTL property package. (c) Data of Agrawal et al.[11] for the total reflux distillation of argon/oxygen at 30 psia. Simulations performed with the REFPROP[67] property package. (d) Data of Shariat and Kunesh[57] for total reflux distillation of cyclohexane/*n*-heptane at 5 psia. Simulations performed with the NRTL property package. Correlations used in this work: Bravo, Rocha, and Fair 1985 (BRF85),[6] Bravo, Rocha, and Fair 1992 (BRF92),[7] and Billet and Schultes.[5]

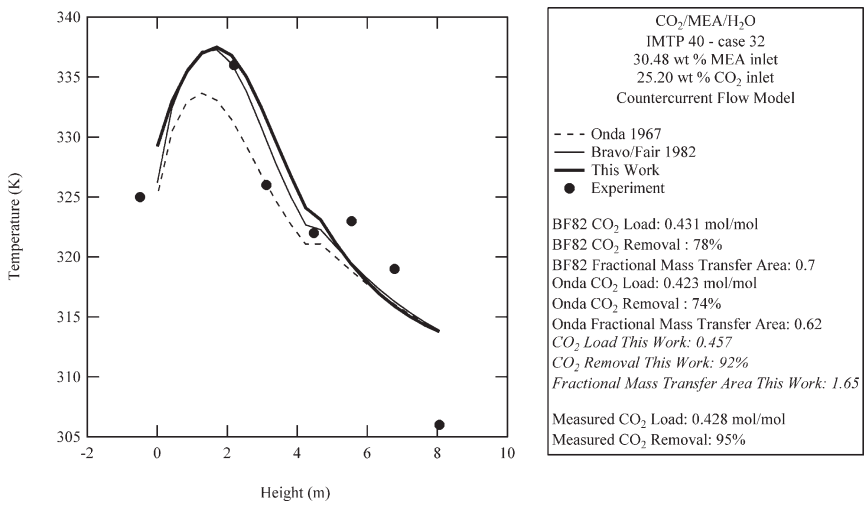

Figure 13. Data of Lawal et al.[40] for the absorption of CO_2 into aqueous MEA (Case 32).

All simulations performed with *Aspen Rate Based Distillation* v7.2 using the VPLUG flow model and the ELECNRTL property package. Correlations used in these calculations: Bravo and Fair[4] and Onda et al.[3]

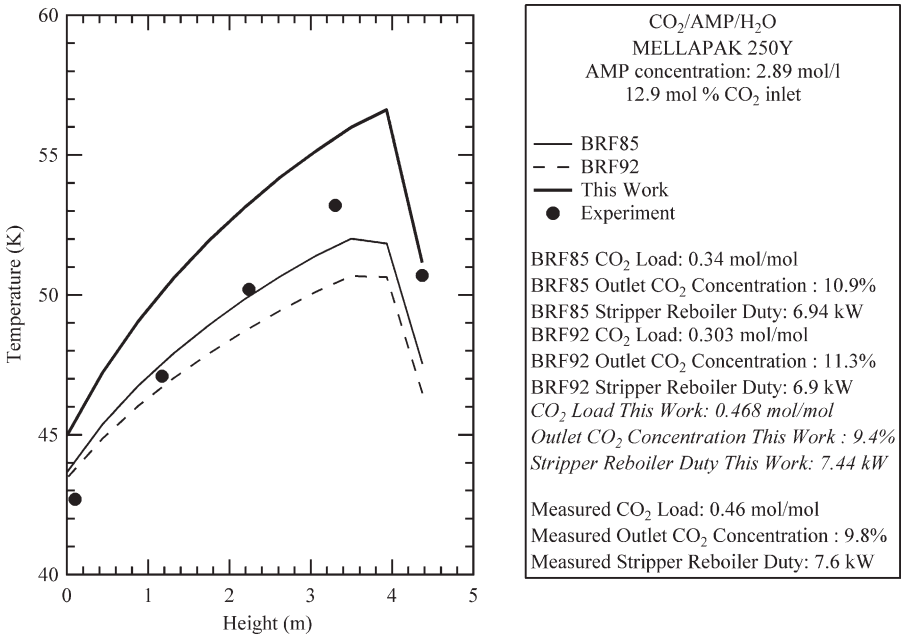

Figure 14. Data of Gabrielson[41] for the absorption of CO_2 into aqueous AMP.

All simulations performed with *Aspen Rate Based Distillation* v7.2 using the VPLUG flow model and the ELECNRTL property package. Correlations used in this work: Bravo, Rocha, and Fair 1985 (BRF85)[6] and Bravo, Rocha, and Fair 1992 (BRF92).[7]

model.[69] The authors[40] found that the experimental column temperature profile for Case 32 could not be matched adequately in their simulations using the nominal flue gas flow rate of 0.13 kg/s. They obtained much closer agreement when the flue gas rate was reduced to 0.11 kg/s. In our simulations, the flue gas flow rate was reduced from the nominally measured value of 0.13 to 0.11 kg/s. Three mass-transfer correlations were examined: (1) the correlation of Onda et al.,[3] (2) the Bravo and Fair correlation of 1982,[4] and (3) the correlation for IMTP developed in this article. Results are summarized in Figure 13. The calculated temperature profiles from all three correlations agree well with the experimentally measured temperature data. Only the new correlation for IMTP developed in this article matches the temperature profile, the rich amine loading, and the outlet flue gas CO_2 concentration simultaneously.

Gabrielson[41] has reported data associated with the absorption of CO_2 by an aqueous solution of 2-amino-2-methyl-1-propanol (AMP) in a column equipped with MELLAPAK 250Y. A typical set of operating conditions is summarized in a brochure produced by Aspen Technology, Inc.[70] Using these operating conditions, both the absorber and the stripper were simulated. Gabrielson's experimental temperature profile data are shown in Figure 14 along with simulated temperature profiles for the BRF85 correlation, the BRF92 correlation, and the mass-transfer correlation for sheet metal structured packings of this article. In our simulations, we used the Aspen v7.0 AMP model.[70] Each correlation produces an acceptable approximation to the actual temperature profile. Gabrielson also reported the CO_2 outlet concentration, the rich solvent CO_2 loading, and the stripper reboiler duty. We also report these in Figure 14 as outputs from each simulation. The correlation of this article reproduces acceptable approximations for all three quantities. Results from the BRF85 and BRF92 correlations show a much lower CO_2 loading than the experimental data.

Shiveler et al.[51] have reported performance data on an H_2S selective absorber retrofitted with MELLAPAKPLUS 252Y sheet metal structured packing. The absorber employs aqueous methyl-diethanolamine (MDEA) as the absorbent. The efficiency of MELLAPAKPLUS 252Y has been reported to be virtually identical to that of MELLAPAK 250Y.[71] The authors reported the absorption selectivity, defined as y_{CO_2}/y_{H_2S}, at the column outlet over the course of several months. Because the inlet gas flow and its composition varied from day to day, three representative design cases were examined for the retrofit. Some of the temporal data collected for the selectivity after the retrofit are shown in Figure 15. Also included are selectivity results for the three reported design cases (labeled in the figure as conditions A, B, and C) calculated with *Aspen Rate Based Distillation* v7.2 using the Aspen v7.0 MDEA model.[72] Only the correlations developed in this article yielded selectivity results in line with those measured. The selectivities calculated with the BRF85,[6] BRF92,[7] and Billet and Schultes[5] correlations were found to be orders of magnitude greater than the experiment values. Also shown in Figure 15 are the calculated CO_2 and H_2S composition profiles for the BRF85 correlation and the new correlation reported here. Note that the CO_2 composition profiles for the two correlations are different by up to a factor of 3. The H_2S profiles differ by a factor of up to 10,000.

deMontigny et al.[52] reported on the absorption of CO_2 by MEA using the metal gauze structured packing DX. We used the correlation developed from BX data, along with the Aspen v7.0 MEA model,[69] to predict the performance of deMontigny's absorber equipped with DX. Figure 16 is a comparison of the measured CO_2 composition profile for run DX-1 with simulated results for the BRF85 correlation and the BX correlation described above. Also included in the figure are the

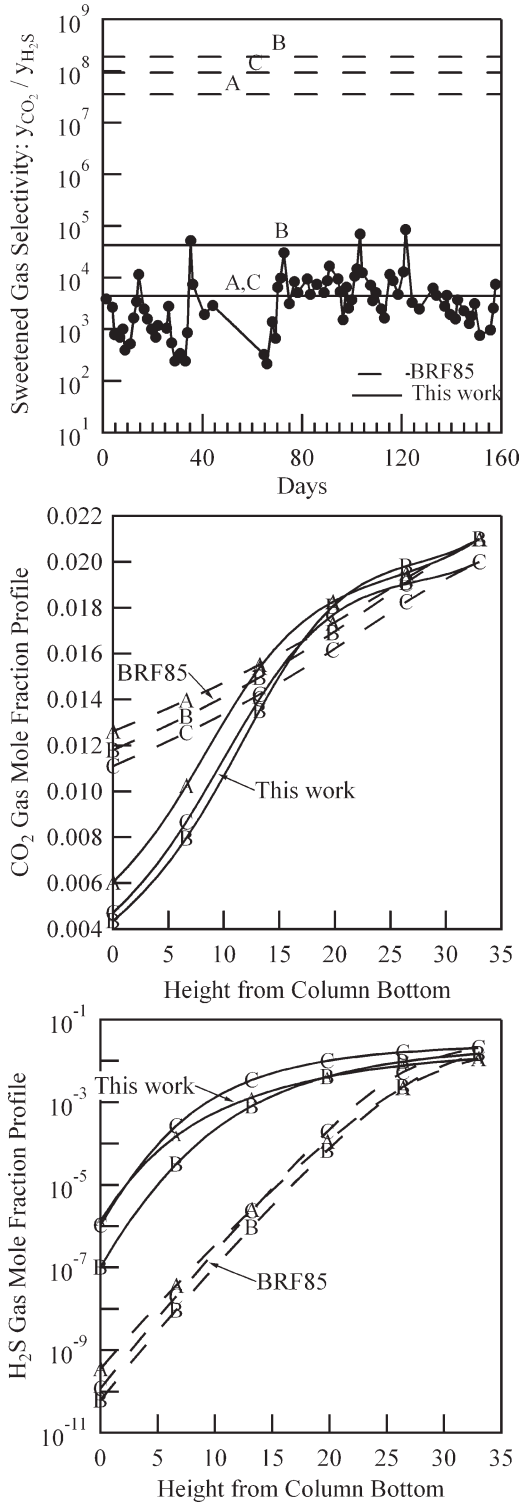

Figure 15. Top: Comparison of the data of Shiveler et al.[51] (-●-) for the CO_2/H_2S selectivity of the outlet flue gas stream with the predicted selectivities calculated using the BRF85 mass-transfer correlation[6] and the correlation presented here for MELLAPAK structured packings.

The A, B, and C labels refer to the three design cases studied by the authors. Middle: Comparison of the calculated CO_2 profiles for the three different design cases. Bottom: Comparison of the calculated H_2S profiles for the three different design cases.

authors' predictions based on their own mass-transfer correlations. The BX correlation of this work successfully reproduces the reported CO_2 composition profile. Even though no other size of gauze packing was included in our BX fit, the BX correlation appears to be applicable to DX and EX also.

Implications: Mass-Transfer Area

The data analysis methodology described in this article results in individual correlating expressions for k_x, k_y, and a_m. The fractional mass-transfer area, a_m/a_d, is the subject of considerable controversy. The Delft correlation[73] and that of Onda et al.[3] predict that the available area for mass transfer approaches the geometrical surface area of the packing exponentially as the liquid rate is increased. The BRF85 correlation[6] for metal gauze structured packings assumes that $a_m = a_d$ under all operating conditions. The correlation of Rocha et al.[42] for a_m is a power law in the liquid rate; a_m/a_d can be greater or less than unity depending upon the other parameters in the correlation. The correlation of Billet and Schultes[5] is also a power law in the liquid rate below the loading point. However, if the surface tension of the liquid is below 30 dyn/cm, then the mass-transfer area is taken to be the geometrical surface area regardless of the nature of the packing's material of construction. For the sake of comparison, effective mass-transfer areas for MELLAPAK 250Y sheet metal structured packing are displayed in Figure 17 for the total reflux distillations of chlorobenzene/ethylbenzene (CB/EB) at 75 and at 760 torr. Clearly, there are noticeable disagreements among the correlations. It might also appear surprising that some correlations, including the new structured packing correlation developed in this article, predict mass-transfer areas well in excess of the dry geometrical surface area of the packing itself. It is important to stress that the interfacial area participating in mass transfer is only loosely correlated to the extent of wetting of the dry packing's geometrical surface area. Additional mass-transfer area can come from the presence of waves on the surface of liquid films flowing over the packing surface, from liquid droplets, or from liquid filaments between packing elements, for example. Incomplete wetting of the packing surface would tend to reduce the mass-transfer area relative to the packing's geometrical surface area. It is more surprising, therefore, that some correlations identify the geometrical surface area of the packing as the maximum amount of interfacial area available for mass transfer.

The most widely used method for measuring a_m is the absorption of CO_2 by aqueous NaOH under conditions where the concentration of CO_2 is low and there is excess $[OH^-]$. The total gas flow can then be treated as constant, and the removal of CO_2 by reaction is well approximated as pseudo-first order. The details of the experimental protocol and the methods of analysis are presented elsewhere.[50,74]

The Danckwerts plot technique[75] simultaneously yields k_L and a_m from mass-transfer experiments. From the measurements of the gas absorption rate at different apparent first-order reaction rate constants, the values of k_L and a_m can be determined using the Danckwerts surface renewal model.

$$\left(\frac{R_A}{m_A c_A V_L}\right)^2 = (k_L a_m)^2 + k_{1,app} D_A a_m^2 \qquad (76)$$

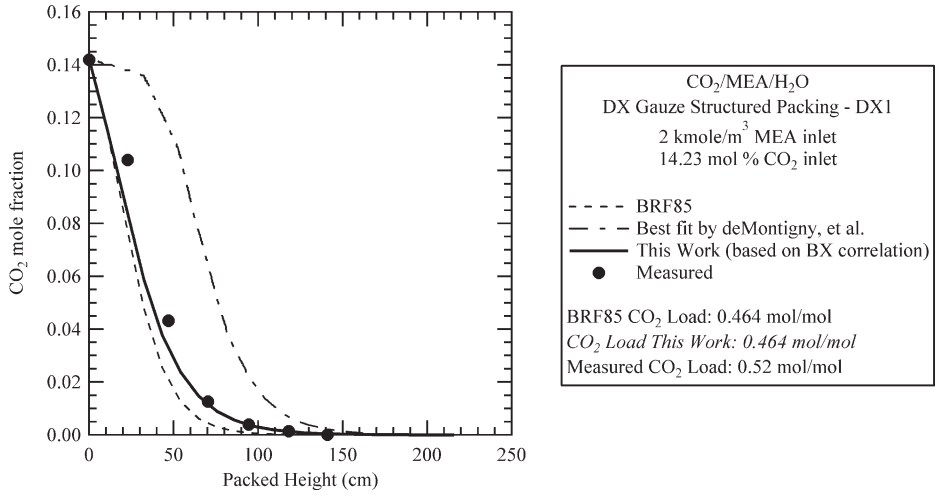

Figure 16. Data of deMontigny et al.[52] for the absorption of CO_2 into aqueous MEA using DX metal gauze structured packing (experiment DX1).

All simulations performed with *Aspen Rate Based Distillation* v7.2 using the VPLUG flow model and the ELECNRTL property package. Correlations used in these calculations: Bravo, Rocha, and Fair 1985[6] and deMontigny et al.[52]

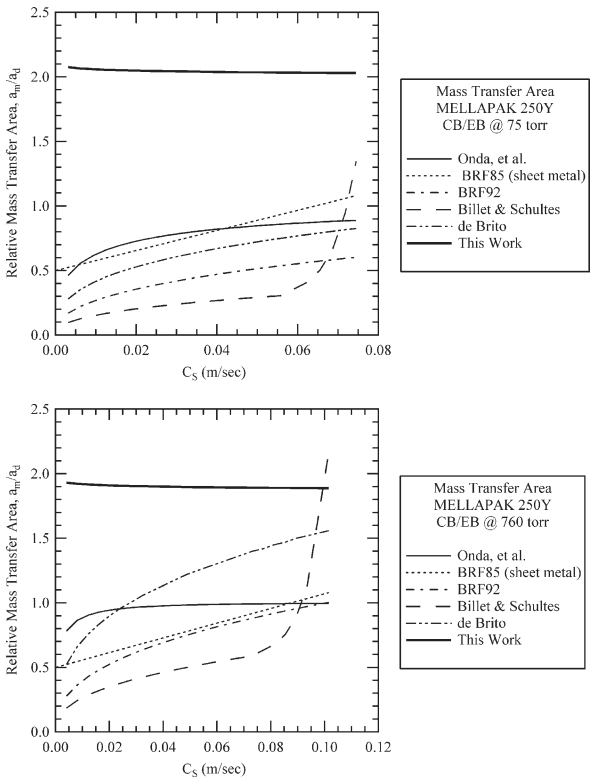

Figure 17. (a) Correlation predictions for the fractional mass-transfer area of MELLAPAK 250Y vs. vapor-corrected superficial vapor velocity, C_S, for the total reflux distillation of chlorobenzene/ethylbenzene at 75 torr; (b) Correlation predictions for the fractional mass-transfer area of MELLAPAK 250Y vs. vapor-corrected superficial vapor velocity, C_S, for the total reflux distillation of chlorobenzene/ethylbenzene at 760 torr.

Correlations used in these calculations: Onda et al.,[3] Bravo, Rocha, and Fair 1985 (BRF85),[6] Bravo, Rocha, and Fair 1992 (BRF92),[7] Billet and Schultes,[5] and de Brito.[60]

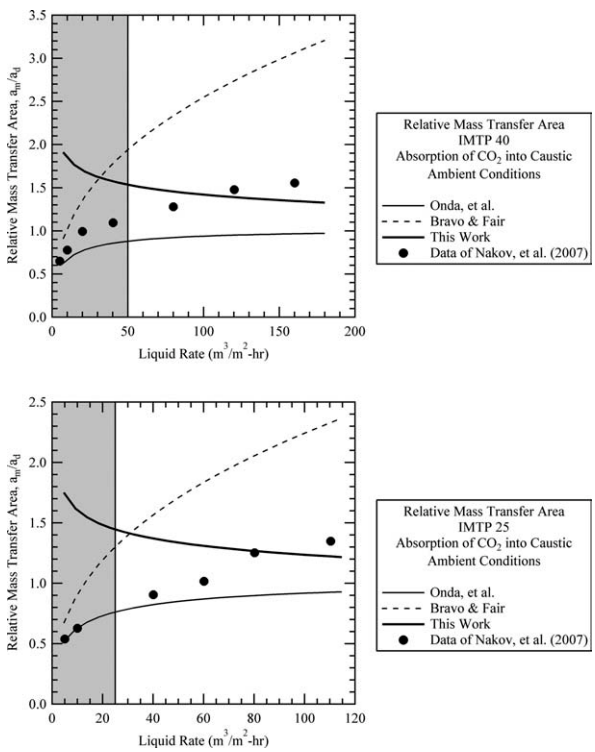

Figure 18. Top: The mass-transfer area of IMTP 40—deduced by Nakov et al.[53] from analysis of data on the absorption of CO_2 into caustic by the method of Danckwerts—compared with mass-transfer area predictions for several correlations; Bottom: The mass-transfer area of IMTP 25—deduced by Nakov et al.[53] from analysis of data on the absorption of CO_2 into caustic by the method of Danckwerts[32]—compared with mass-transfer area predictions for several correlations.

Correlations used in these calculations: Bravo and Fair[4] and Onda et al.[3]

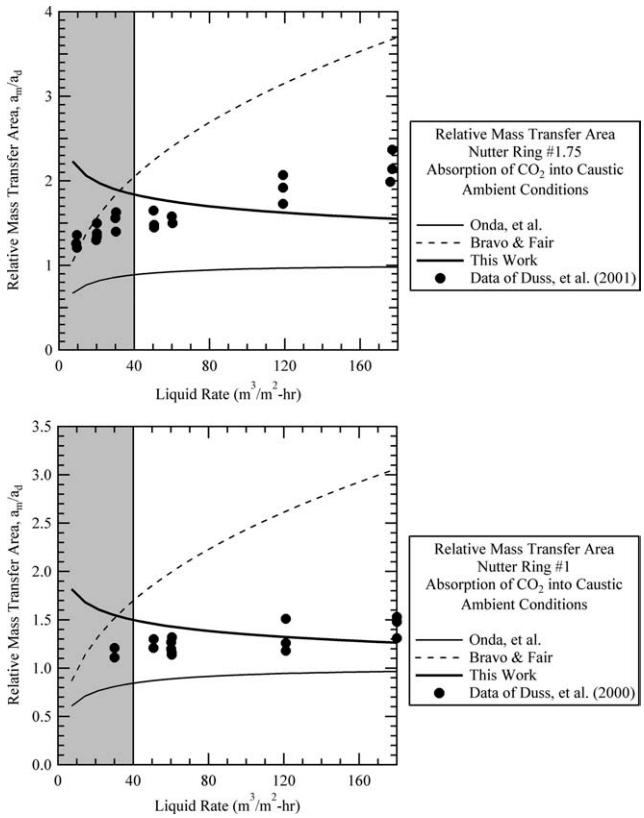

Figure 19. Top: The mass-transfer area of Nutter ring #1.75—deduced by Duss et al.[62] from analysis of data on the absorption of CO_2 into caustic by the method of Danckwerts—compared with mass-transfer area predictions for several correlations; Bottom: The mass-transfer area of Nutter ring #1—deduced by Duss et al.[54] from analysis of data on the absorption of CO_2 into caustic by the method of Danckwerts[32]—compared with mass-transfer area predictions for several correlations.

Correlations used in these calculations: Bravo and Fair[4] and Onda et al.[3]

Equation 76 is in the form of a straight line with the abscissa being the apparent pseudo-first-order rate constant, $k_{1,\mathrm{app}}$. In the case of CO_2 absorption into caustic $k_{1,\mathrm{app}} = k_{\mathrm{OH}}^{-}[\mathrm{OH}^-]$.

The method employed by Tsai et al.[74] equates the two material balances obtained by considering material exchange starting from the vapor side and then from the liquid side. These balances yield the following relation between the physical liquid-side mass-transfer coefficient, k_L, and the gas-side mass-transfer coefficient, k_G

$$\frac{k_L}{H_{CO_2}}\sqrt{1+\frac{k_{OH^-}[OH^-]D_{L,CO_2}}{k_L^2}}=\frac{k_L}{H_{CO_2}}\sqrt{1+Ha^2}=k_G \quad (77)$$

when the Hatta number is large relative to unity, then the following simplification can be made

$$\frac{1}{H_{CO_2}}\sqrt{k_{OH^-}[OH^-]D_{L,CO_2}}\cong k_G \quad \mathrm{Ha}\gg 1 \quad (78)$$

The authors state that the approximation given in Eq. 78 introduces errors less than or equal to 6% in the calculation of a_m for the Hatta numbers encountered in their investigations when the correlation of Rocha et al.[42] is used to estimate k_L. However, it is known that estimates for k_L based on correlations found in the literature can vary significantly from one another.[64] It is not clear, therefore, that the approximation of Eq. 78 is warranted nor is it clear what the actual uncertainties are in the reported values of a_m when this approach is used.

Nakov et al.,[53] Kolev et al.,[61] and Duss et al.[54,62] used the Danckwerts technique to analyze the CO_2 absorption into aqueous NaOH for metal and plastic Raschig Super-Rings, metal IMTP, metal Nutter rings, and plastic Ralu-Flow rings. These data give us the opportunity to contrast the IMTP mass-transfer area correlation predictions of Eq. 69 with experimentally measured values for the mass-transfer area. Figure 18 compares the data of Nakov et al.[53] for the variation of the effective mass-transfer areas of IMTP 40 and IMTP 25 with liquid load to calculated variations based on the Onda correlation,[3] the correlation of Bravo and Fair,[4] and the IMTP area correlation developed in this article (Eq. 69). Figure 19 is a similar comparison using the data of Duss et al.[62] for Nutter rings #1.75 and #1 (Nutter rings are geometrically very similar to IMTP). A potential weakness of the new interfacial-area correlations for random packings reported in this article is the fact that they predict that the interfacial area for mass transfer increases as the liquid load goes to zero. However, one must recall that efficiency data in the low liquid rate regime, where there is significant

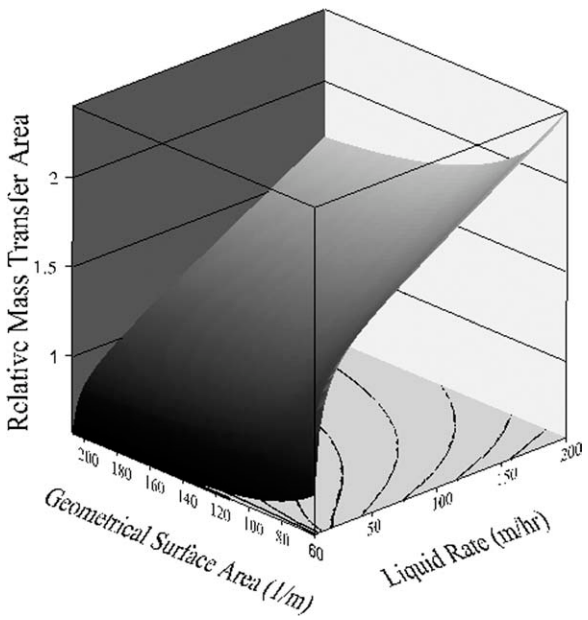

Figure 20. Smoothed and interpolated data of Nakov et al.[53] for the mass-transfer area of the IMTP family of random packings as a function of their geometrical surface area and the liquid load.

underwetting of the packing's geometrical surface and an upturn in the ⟨HETP⟩, were excluded from consideration at the outset. Therefore, the upturns in the predicted interfacial area for mass transfer at low liquid rates observed with these correlations are an artifact of the assumptions made at the outset in developing them. In short, these correlations should not be applied below minimum liquid rate expected for good performance of the packing—typically about 30–40% of flood.

In Figure 20, the mass-transfer area data of Nakov et al.[53] for the various IMTP sizes have been smoothed and interpolated to create a three-dimensional portrayal of the mass-transfer area as a function of the packing's dry surface area and of the liquid flow rate. The figure implies that the mass-transfer area for IMTP falls below the geometrical surface area for smaller packing sizes at low liquid flow rates. Conversely, the area participating in mass transfer greatly exceeds the dry packing surface area for larger packing sizes at higher liquid flow rates.

Conclusions

Mass-transfer coefficient/effective surface-area correlations for metal Pall rings, metal IMTP, sheet metal structured packings of the MELLAPAK/FLEXIPAC type, and metal gauze packings in the X configuration have been developed using a new fitting procedure based on dimensional analysis combined with concurrent fitting of binary HETP data and acid gas absorption data. The procedure and the resulting new correlations provide better estimates of mass-transfer-related quantities over a broader range of packing sizes and unit operations than do other public-domain correlations. Used in rate-based calculations for columns, these correlations form part of the underlying equations for accurate prediction of equipment performance. The improved mass-transfer correlations are particularly instrumental in the reliability of rate-based column calculations of chemical systems such as CO_2 capture with amines as chemical absorbents.

Notation

Symbols

a_d = dry specific packing area (m^2/m^3)
a_m = specific packing area participating in mass transfer (m^2/m^3)
A_L = front factor on the liquid-side mass-transfer correlation (dimensionless)
A_M = front factor on the mass-transfer area correlation (dimensionless)
A_V = front factor on the vapor-side mass-transfer correlation (dimensionless)
Bo = Bond number (dimensionless)
c_L = liquid-phase molar concentration (mol/m^3)
c_V = vapor-phase molar concentration (mol/m^3)
D = column diameter (m)
D_L = liquid-phase binary diffusivity (m^2/s)
D_V = vapor-phase binary diffusivity (m^2/s)
C_S = density-corrected superficial vapor velocity = $v_V\sqrt{\rho_V/(\rho_L-\rho_V)}$ (m/sec)
C_x = correction factor defined by Eq. 27 (dimensionless)
C_y = correction factor defined by Eq. 26 (dimensionless)
d_e = equivalent diameter = $4\varepsilon/a_d$ (m)
F_S = $v_V\sqrt{\rho_V}$ ($Pa^{1/2}$)
Fr_L = liquid-phase Froude number (dimensionless)
g = acceleration of gravity (m/s^2)
G = superficial molar vapor flux (mol/m^2 s)
HETP = point or local Height Equivalent to a Theoretical Plate (m)
⟨HETP⟩ = column average Height Equivalent to a Theoretical Plate (m)
k_x = liquid-side mass-transfer coefficient based on mole fraction driving force (mol/m^2 s)
k_y = vapor-side mass-transfer coefficient based on mole fraction driving force (mol/m^2 s)
K_{Oy} = overall mass-transfer coefficient = $k_xk_y/(k_x + mk_y)$ (mol/m^2 s)
L = superficial molar liquid flux (mol/m^2 s)
m = slope of the y–x equilibrium curve for binary systems: $\frac{y_{n-1}-y_n}{x_{n-1}-x_n}$ or $\left(\frac{\partial y}{\partial x}\right)_P$
N = total number of equilibrium stages (dimensionless)
N_A = molar flux of material across an interface (mol/m^2 s)
Re_L = liquid-phase Reynolds number (dimensionless)
Re_V = vapor-phase Reynolds number (dimensionless)
Sc_L = liquid-phase Schmidt number (dimensionless)
Sc_V = vapor-phase Schmidt number (dimensionless)
Sh_L = liquid-phase Sherwood number (dimensionless)
Sh_V = vapor-phase Sherwood number (dimensionless)
v_L = superficial liquid velocity (m/s)
v_V = superficial vapor velocity (m/s)
We_L = liquid-phase Weber number (dimensionless)
x = liquid-phase mole fraction (dimensionless)
y = vapor-phase mole fraction (dimensionless)
α = binary relative volatility (dimensionless)
λ = mG/L (dimensionless)
μ_L = liquid viscosity (kg/m s)
μ_V = vapor viscosity (kg/m s)
ρ_L = liquid density (kg/m^3)
ρ_V = vapor density (kg/m^3)

Nomenclature

AMP = 2-amino-2-methyl-1-propanol
BF82 = transfer coefficient/interfacial-area correlation given in Ref. 4
BRF85 = mass-transfer coefficient/interfacial-area correlation given in Ref. 6
BRF92 = mass-transfer coefficient/interfacial-area correlation given in Ref. 7
BX = metal gauze structured packing with a geometrical surface area of ~500 m^2/m^3 and a corrugation inclination angle of 30° from the vertical
CB = chlorobenzene
DX = metal gauze structured packing with a geometrical surface area of ~900 m^2/m^3 and a corrugation inclination angle of 30° from the vertical.
EB = ethylbenzene
MDEA = methyl-diethanolamine
MEA = monoethanolamine

Literature Cited

1. Adler S, Beaver E, Bryan P, Robinson S, Watson J. *Vision 2020: 2000 Separations Roadmap*. New York: American Institute of Chemical Engineers, 2000; ISBN 0–8169-0832-X.
2. Aspen Technology, Inc. Aspen rate based distillation. Aspen Technology website. 2010. Available at: www.aspentech.com/products/aspen-ratesep.cfm. Accessed June 24, 2010.
3. Onda K, Takeuchi H, Koyama Y. Effect of packing materials on the wetted surface area. *Kagaku Kogaku*. 1967;31:126–134.
4. Bravo JL, Fair JR. Generalized correlation for massttransfer in packed distillation columns. *Ind Eng Chem Process Des Dev*. 1982;21:162–170.
5. Billett R, Schultes M. Prediction of mass transfer columns with dumped and arranged packings: updated summary of the calculation method of Billett and Schultes. *Trans Inst Chem Eng*. 1999;77A:498–504.
6. Bravo JL, Rocha JA, Fair JR. Mass transfer in gauze packings. *Hydrocarbon Process*. 1985;64:91.
7. Bravo JL, Rocha JA, Fair JR. A comprehensive model for the performance of columns containing structured packings. *IChemE Symposium Series No. 128*. 1992;128:A439.
8. Kister HZ. *Distillation Design*. New York: McGraw-Hill, 1992.
9. Schultes M. Raschig super-ring: a new 4th generation packing. *Chem Eng Res Des*. 2003;81:48–57.

10. Fitz CW, Kunesh JG, Shariat A. Performance of structured packing in a commercial-scale column at pressures of 0.02–27.6 bar. *Ind Eng Chem Res*. 1999;38:512–518.
11. Agrawal R, Woodward DW, Ludwig KA, Bennett DL. Impact of low pressure drop structure packing on air distillation. Paper presented at *Distillation and Absorption: IChemE Symposium Series 128*. Maastricht, The Netherlands, 1992.
12. Kean JA, Turner HM, Price BC. Structured packing proven superior for TEG gas drying. *Oil Gas J*. 1991;89:41–46.
13. Sherwood TK. *Absorption and Extraction*. New York: McGraw-Hill, 1937.
14. Taylor R, Krishna R. *Multicomponent Mass Transfer*. New York: Wiley, 1993.
15. Treybal RE. *Mass-Transfer Operations*, 3rd ed. New York: McGraw-Hill, 1980.
16. Bolles WL, Fair JR. Improved mass-transfer model enhances packed-column design. *Chem Eng*. July 12, 1982:109–116.
17. Wu KY, Chen GK. Large-scale pilot columns and packed column scale-up. *IChemE Symp Ser*. 1987;104:B225–B245.
18. Doherty MF, Malone MF. *Conceptual Design of Distillation Systems*. New York: McGraw-Hill, 2001.
19. Hanley B. Calculation of the HETP at total reflux: generalization of the Fenske equation. Paper presented at *2001 AIChE Annual Meeting*, Reno, 2001.
20. Eckert JS, Foote EH, Walter LF. What affects packing performance? *Chem Eng Prog*. 1966;62:59.
21. Billet R. Recent investigations of metal pall rings. *Chem Eng Prog*. 1967;63:53.
22. Gualito JJ, Cerino FJ, Cardenas JC, Rocha JA. Design method for distillation columns filled with metallic, ceramic, or plastic structured packings. *Ind Eng Chem Res*. 1997;36:1747–1757.
23. Murch DP. Height of equivalent theoretical plate in packed fractionation columns. *Ind Eng Chem*. 1953;45:2616–2621.
24. Bolles WL, Fair JR. Performance and design of packed distillation columns. *IChemE Symp Ser*. 1979;56:35–89.
25. Barenblatt GI. *Scaling, Self-Similarity, and Intermediate Asymptotics*. Cambridge: Cambridge University Press, 1996.
26. Krug RR. Fitting data to dimensionless groups. *Ind Eng Chem Res Fundam*. 1978;17:306–308.
27. Krug RR, Hunter WG, Grieger RA. Enthalpy-entropy compensation. I. Some fundamental statistical problems associated with the analysis of van't Hoff and Arrhenius data. *J Phys Chem*. 1976;80:2335–2341.
28. Churchill SW. Critique of the classical algebraic analogies between heat, mass, and momentum transfer. *Ind Eng Chem Res*. 1997;36:3866–3878.
29. Chilton TH, Colburn AP. Mass transfer (absorption) coefficients: predictions from data on heat transfer and fluid friction. *Ind Eng Chem*. 1934;26:1183–1187.
30. Bird RB, Stewart WE, Lightfoot EN. *Transport Phenomena*, 2nd ed. New York: Wiley, 2002.
31. Higbie R. The rate of absorption of a pure gas into a still liquid during short periods of exposure. *Trans Am Inst Chem Eng*. 1935; 31:365.
32. Danckwerts PV. Significance of liquid film coefficients in gas absorption. *AIChE J*. 1957;3:1460.
33. Sherwood TK, Holloway FA. Performance of packed towers-liquid film data for several packings. *Trans Am Inst Chem Eng*. 1940;36:39.
34. Koch HA, Stutzman LF, Blum HA, Hutchings HA. Liquid transfer coefficients for carbon dioxide air-water system. *Chem Eng Prog*. 1949;45:677.
35. Van Krevelin DW, Hoftijzer PJ. Studies of gas absorption. I. Liquid film resistance to gas absorption in scrubbers. *Receuil des Trav Chim des Pays-Bas*. 1947;66:49–70.
36. Potnis SV, Lenz TG. Dimensionless mass-transfer correlations for packed-bed liquid-desiccant contactors. *Ind Eng Chem Res*. 1996; 35:4185–4193.
37. Shetty S, Cerro RL. Fundamental liquid flow correlations for the computation of design parameters for ordered packings. *Ind Eng Chem Res*. 1997;36:771–783.
38. Bennett DL. Optimize distillation columns. II. Packed columns. *Chem Eng Prog*. May, 2000:27–34.
39. McNulty K, Hsieh CL. Hydraulic performance and efficiency of Koch flexipac structured packings. Paper presented at *1982 AIChE Annual Meeting*, Los Angeles, 1982.
40. Lawal A, Wang M, Stephenson P, Yeung H. Dynamic modelling of CO_2 absorption for post combustion capture in coal-fired power plants. *Fuel*. 2009;88:2455–2462.
41. Gabrielsen J. CO_2 capture from coal fired power plants. PhD Thesis, Technical University of Denmark, 2007.
42. Rocha JA, Bravo JL, Fair JR. Distillation columns containing structured packings: a comprehensive model for their performance. II. Mass-transfer model. *Ind Eng Chem Res*. 1996;35:1660–1667.
43. Wagner I, Stichlmair J, Fair JR. Mass transfer in beds of modern, high-efficiency random packings. *Ind Eng Chem Res*. 1997;36:227–237.
44. Rukovena JF, Niknafs H, Hausch G. Mass transfer and hydraulic details on Intalox PhD packing. Paper presented at *Distillation and Absorption 2002 Proceedings*, Baden-baden, Germany, 2002:paper 6–9.
45. Koshy TD, Rukovena F. Available at: http://www.cheresources.com/distillationmodel.pdf. CheResources.com. http://www.cheresources.-com. Accessed April 19, 2010.
46. Ludwig EE. *Applied Process Design for Chemical snd Petrochemical Plants, Vol. 2*, 3rd ed. Houston: Gulf Professional Publishing, 1997.
47. Nooijen JL, Kusters KA, Pek JJB. The performance of packing in high pressure distillation applications. *IChemE Symp Ser*. 1997; 142:885.
48. Kister HZ, Mathias PM, Steinmeier DE, Penney WR, Crocker BB, Fair JR. *Equipment for distillation, gas absorption, phase dispersion, and phase separation*. In: Green DW, Perry RH, editors. *Perry's Chemical Engineers' Handbook*, 8th ed. New York: McGraw-Hill, 2008:65–67.
49. Cai T, Chen GX. Structured packing performance. Paper presented at *First China-USA Joint Conference on Distillation Technology*, Tianjin, 2004;2455–2462.
50. Kolev N. *Packed Bed Columns for Absorption, Desorption, Rectification and Direct Heat Transfer*. London: Elsevier, 2006.
51. Shiveler G, Solis GS, Gonzalez LHP, Bueno ML. Retrofit of a H_2S selective amine absorber using MellapakPlus structured packing. Paper presented at *2005 Spring AIChE Meeting*, Atlanta, 2005.
52. deMontigny D, Aboudheir A, Tontiwachwuthikul P. Modelling the performance of a CO_2 absorber containing structured packing. *Ind Eng Chem Res*. 2006;45:2594–2600.
53. Nakov S, Kolev N, Ljutzkanov L, Kolev D. Comparison of the effective area of some highly effective packings. *Chem Eng Process*. 2007;46:1385–1390.
54. Duss M, Meierhofer H, Bornio P. Bestimmung der Effektiven Stoffaustauschflächen bei hoher Flüssigkeitsbelastung für Nutter-Ringe. *Chem Ing Tech*. 2000;72:1053.
55. Wang S, Zeng Z, Li X. Investigation on rectifying characteristics of two new tower packings. *Huagong Xuebao*. 1990;41:187–194, (in Chinese).
56. Newsfront. Boosting tower performance by more than a trickle. *Chem Eng*. May 27, 1985:187–194.
57. Shariat A, Kunesh JG. Packing efficiency testing on a commercial scale with good (and not so good) reflux distribution. *Ind Eng Chem Res*. 1995;34:1273–1279.
58. Bennett K, Pilling M. Efficiency benefits of high performance structured packings. Paper presented at *Texas Technology Showcase 2003, D2: Separations or Distillation Technologies*, Houston, 2003.
59. Fair JR, Seibert AF, Behrens M, Saraber PP, Olujić Ž. Structured packing performance—experimental evaluation of two predictive models. *Ind Eng Chem Res*. 2000;39:1788–1796.
60. de Brito MH. Gas absorption experiments in a pilot column with the Sulzer structured packing MELLAPAK. PhD Thesis, Lausanne: Ecole Polytechnique Federale de Lausanne, 1991.
61. Kolev N, Nakov S, Ljutzkanov L, Kolev D. Effective area of a highly effective random packing. *Chem Eng Process*. 2006;45:429–436.
62. Duss M, Meierhofer H, Nutter DE. Effective interfacial area and liquid holdup of Nutter rings at high liquid loads. *Chem Eng Technol*. 2001;24:716–723.
63. Gabrielsen J, Svendsen H, Michelsen ML, Stenby EH, Kontogeorgis GM. Experimental validation of a rate-based model for CO_2 capture using an AMP solution. *Chem Eng Sci*. 2007;62:2397–2413.
64. Wang GQ, Yuan XG, Yu KT. Review of mass-transfer correlations for packed columns. *Ind Eng Chem Res*. 2005;44:8715–8729.
65. Renon H, Prausnitz JM. Local compositions in thermodynamic excess functions for liquid mixtures. *AIChE J*. 1968;14:135–144.
66. Chen CC, Britt HI, Boston JF, Evans LB. Local composition model for excess Gibbs energy of electrolyte systems. *AIChE J*. 1982;28:588–596.
67. National Institute of Science and Technology. NIST Refprop description. NIST website. November 19, 2009. Available at: www.nist.gov/cstl/properties/fluids_modeling/refprop.cfm. Accessed June 24, 2010.

68. Zhang Y, Chen H, Chen CC, Plaza JM, Dugas R, Rochelle GT. Rate-based process modeling study of CO_2 capture with aqueous monoethanolamine solution. *Ind Eng Chem Res*. 2009;48:9233–9246.
69. Aspen Technology, Inc. *Rate-Based Model of the CO_2 Capture Process by MEA using Aspen Plus*. Burlington, MA: Aspen Technology, Inc., 2008.
70. Aspen Technology, Inc. *Rate-Based Model of the CO_2 Capture Process by AMP using Aspen Plus*. Burlington, MA: Aspen Technology, Inc., 2008.
71. Sulzer Chemtech. *Structured Packings for Distillation, Absorption, and Reactive Distillation*, *Vol 22.13.06.40*.
72. Aspen Technology, Inc. *Rate-Based Model of the CO_2 Capture Process by MDEA using Aspen Plus*. Burlington, MA: Aspen Technology, Inc., 2008.
73. Olujic Z, Kamerbeek AB, de Graauw JA. Corrugation geometry based model for efficiency of structured distillation packing. *Chem Eng Proc*. 1999;38:683.
74. Tsai RE, Schultheiss P, Kettner A, Rochelle GT, Lewis JC, Seibert AF, Eldridge RB. Influence of surface tension on effective packing area. *Ind Eng Chem Res*. 2008;47: 1253–1260.
75. Cents AHG, Brilman DWF, Versteeg GF. CO_2 absorption in carbonate/bicarbonate solutions: the Danckwerts-criterion revisited. *Chem Eng Sci*. 2005;60:5830–5835.

Appendix A: Derivation of Eq. 20

The Fenske equation for a separation involving a binary system with constant relative volatility in a column operating at total reflux can be written as

$$\left(\frac{x_j}{1-x_j}\right) = \alpha^{(j-i)}\left(\frac{x_i}{1-x_i}\right) \tag{A1}$$

where x_i is the liquid composition on stage "i," x_j is the liquid composition on stage "j," α is the relative volatility, and $\Delta n = (j - i)$ is the number of stages. If we imagine that tray numbering is continuous rather than discrete, then it is possible to write the equation above, for a small change in composition, as

$$\left(\frac{x+\Delta x}{1-x-\Delta x}\right) = \alpha^{\Delta n}\left(\frac{x}{1-x}\right) \tag{A2}$$

which can be rearranged to give

$$\left(1+\frac{\Delta x}{x}\right) = \alpha^{\Delta n}\left(1+\frac{\Delta x}{1-x}\right) \tag{A3}$$

which can then be further manipulated to yield

$$\ln\left(1+\frac{\Delta x}{x}\right) - \ln\left(1-\frac{\Delta x}{1-x}\right) = \Delta n \ln(\alpha) \tag{A4}$$

At this point recall that

$$\ln(1+\varepsilon) \approx \varepsilon$$
$$\ln(1-\varepsilon) \approx -\varepsilon$$

Therefore, for a very small change in composition, Eq. A4 can be approximated as

$$\frac{\Delta x}{x} + \frac{\Delta x}{1-x} \cong \Delta n \ln(\alpha) \tag{A5}$$

which can finally be rearranged to

$$\Delta n = \frac{\Delta x}{x(1-x)\ln(\alpha)} \tag{A6}$$

In the limit of an infinitesimally small composition change, Eq. A6 becomes

$$\lim_{\Delta x \to 0} \frac{\Delta n}{\Delta x} = \frac{dn}{dx} = \frac{1}{x(1-x)\ln(\alpha(x))} \tag{A7}$$

where α has been replaced by $\alpha(x)$, the point relative volatility for composition "x." The number of stages for a finite level of separation between the top and bottom of the column is therefore approximated by the integral

$$\int_0^{N+1} dn = N + 1 \cong \int_{x_b}^{x_t} \frac{dx}{x(1-x)\ln[\alpha(x)]} \tag{A8}$$

Equations A7 and A8 correspond to Eqs. 19 and 20 of the text.

Equation A7 can also be derived by direct differentiation of the Fenske equation

$$\left(\frac{x}{1-x}\right) = \alpha^n\left(\frac{x_b}{1-x_b}\right) \tag{A9}$$

(where x_b is the composition at the bottom of the column) with the assumption that

$$\frac{d(\ln(\alpha))}{dx} = \frac{1}{\alpha}\frac{d(\alpha)}{dx} \cong 0 \tag{A10}$$

Appendix B: Derivation of Eq. 24

For any binary system at constant pressure, the vapor/liquid equilibrium relationship can be expressed as

$$y(x) = \frac{\alpha(x)x}{1+(\alpha(x)-1)x} \tag{B1}$$

The slope of the equilibrium curve is, therefore, given by

$$m(x) = \frac{dy}{dx} = \frac{\alpha(x) + x(1-x)\frac{d\alpha}{dx}}{[1+(\alpha(x)-1)x]^2} \tag{B2}$$

In Appendix A, we showed that $d\alpha/dx \approx 0$ should be satisfied when deriving a continuous-stage version of the Fenske equation. Therefore

$$m(x) = \frac{dy}{dx} \simeq \frac{\alpha(x)}{[1+(\alpha(x)-1)x]^2} \tag{B3}$$

to the same level of approximation.

Appendix C: Curve Fitting Total Reflux Data

The datasets used in this article consisted of experiments performed exclusively at total reflux. Total reflux implies that

$$\rho_L v_L \cong \rho_v v_v \tag{C1}$$

which, in turn, implies that

$$Re_{\mathrm{L}} = \frac{d_e v_{\mathrm{L}} \rho_{\mathrm{L}}}{\mu_{\mathrm{L}}} \cong \left(\frac{d_{\mathrm{e}} v_{\mathrm{v}} \rho_{\mathrm{v}}}{\mu_{\mathrm{v}}}\right)\left(\frac{\mu_{\mathrm{v}}}{\mu_{\mathrm{L}}}\right) \cong (Re_{\mathrm{v}})\left(\frac{\mu_{\mathrm{v}}}{\mu_{\mathrm{L}}}\right) \tag{C2}$$

Substitution of (C2) into Eq. 45 (with appropriate coefficients fixed as described in the text) leads to the following relationship

$$\langle \mathrm{HETP} \rangle = \frac{Gd_{\mathrm{e}}}{\left(A_{\mathrm{M}}\left(\frac{\rho_{\mathrm{V}}}{\rho_{\mathrm{L}}}\right)^{\mathrm{A}}\left(\frac{\mu_{\mathrm{V}}}{\mu_{\mathrm{L}}}\right)^{\mathrm{B+x}}(Fr_{\mathrm{L}}^{\Lambda})(We_{\mathrm{L}}^{\mathrm{E}})(Re_{\mathrm{V}}^{\Phi+X+1})a_{\mathrm{d}}\right)} \times \left(\frac{C_{\mathrm{y}}}{A'_{\mathrm{V}} Sc_{\mathrm{V}}^{1/3} c_{\mathrm{V}} D_{\mathrm{v}}} + \frac{C_{\mathrm{x}}}{\left(\frac{\mu_{\mathrm{V}}}{\mu_{\mathrm{L}}}\right) Sc_{\mathrm{L}}^{1/3} c_1 D_{\mathrm{L}}}\right) \tag{C3}$$

which can be rewritten as

$$\langle \mathrm{HETP} \rangle = \frac{Gd_{\mathrm{e}}}{\left(A'_{\mathrm{M}}\left(\frac{\rho_{\mathrm{V}}}{\rho_{\mathrm{L}}}\right)^{\mathrm{A}}\left(\frac{\mu_{\mathrm{V}}}{\mu_{\mathrm{L}}}\right)^{\mathrm{B'}}(Fr_{\mathrm{L}}^{\Lambda})(We_{\mathrm{L}}^{\mathrm{E}})(Re_{\mathrm{V}}^{\Phi})a_{\mathrm{d}}\right)} \times \left(\frac{C_{\mathrm{y}}}{A'_{\mathrm{V}} Sc_{\mathrm{V}}^{1/3} c_{\mathrm{V}} D_{\mathrm{v}}} + \frac{C_{\mathrm{x}}}{Sc_{\mathrm{L}}^{1/3} c_1 D_{\mathrm{L}}\left(\frac{\mu_{\mathrm{V}}}{\mu_{\mathrm{L}}}\right)}\right) \tag{C4}$$

where $\Phi' = \Phi + X + 1$ and $B' = B + X$.

Thus, curve-fitted estimates of the individual coefficients B, X, and Φ are subjected to a large degree uncertainty. The observations above suggest that experimenters perform several packing efficiency tests at conditions other than total reflux, so that the uncertainties in Φ, X, and B can be reduced.

Manuscript received Jun. 29, 2010, and revision received Jan. 4, 2011.